ABSTRACT

GUPTA, GAURAV. Investigation of Vector Antennas and their Applications. (Under the direction of Prof. Gianluca Lazzi).

The use of multiple antennas at the transmitter and receiver can significantly improve the performance of wireless communication systems. In recent years, there has been a lot of interest in vector or multi-polarized antennas that can provide a compact alternative to spatial array antennas that are conventionally used in multiple antenna systems. In this dissertation, we investigate the performance benefits (like degrees of freedom, channel capacity, mean signal energy etc) that vector antennas can provide when used in two types of multiple antenna systems: multiple-input multiple-output (MIMO) communication systems and frequency selective surfaces (FSSs).

We first characterize the degrees of freedom of fields produced by a linear array of tri-polarized antennas in a MIMO communication system. Using signal space concepts, we derive a sufficient condition for three-fold increase in the degrees of freedom for a system that uses tri-polarized antennas as compared to a system that uses uni-polarized antennas. We show that this condition holds true for three different types of antenna elements: infinitesimally small antennas, finite length dipoles and long wire traveling wave antennas. Since the degrees of freedom determines the slope of channel capacity vs. signal-to-noise ratio (SNR) curve at high SNRs, this result indicates the possibility of increasing channel capacity using tri-polarized antennas.

We then consider practical aspects of vector antenna design. Using simulations, we design two types of vector antennas, one with half-wavelength dipole elements and second with meanderline traveling wave antenna elements. These vector antennas were then fabricated and tested to verify that they provide low return loss and inter-element mutual coupling. We calculated the channel capacity of the system obtained by arranging these antennas in a linear array configuration. As predicted by the degrees of freedom result, we found that the capacity increased three-fold in both cases as compared to an analogous system with uni-polarized antennas.

Finally, we consider the use of vector antennas as unit elements of FSSs. FSSs act as filters to the incident electromagnetic waves based on their frequency and polarization. The reflected signal acts as a signature and can be used to detect the presence of FSS. We design and integrate two prototypes of vector antennas on fabric. Using a monostatic transceiver, we show that FSSs that use vector antennas provide a higher reflected mean-signal-energy (MSE) compared to FSSs that use uni-polarized antennas. We also found that the use of vector antennas makes the FSS more robust to misalignment with the transceiver.

Investigation of Vector Antennas and their Applications

by
Gaurav Gupta

A dissertation submitted to the Graduate Faculty of
North Carolina State University
in partial fullfillment of the
requirements for the Degree of
Doctor of Philosophy

Electrical Engineering

Raleigh, North Carolina

2008

APPROVED BY:

Dr. J. Keith Townsend	Dr. Robert T. Buche
Dr. Gianluca Lazzi Chair of Advisory Committee	Dr. Brian L. Hughes

DEDICATION

To my parents

BIOGRAPHY

Gaurav Gupta received the B. Tech. degree in Electronics and Communications Engineering from Indian Institute of Technology - Guwahati, India in 2004. In August 2004, he started his Ph. D. degree study at North Carolina State University under the guidance of Prof. Gianluca Lazzi. He defended his dissertation in August 2008. His research interests include Antenna Design, MIMO Wireless Communication Systems and Circuit Design.

ACKNOWLEDGMENTS

It has been an enlightening experience to work under the guidance of Dr. Gianluca Lazzi. I sincerely thank him for his keen insight and continuous encouragement throughout the course of my study. I would also like to express my gratitude to Dr. Brian Hughes. His elegant problem solving skills and critical approach towards research have enabled me to present my results in a very rigorous form. I am also specially thankful to Dr. Keith Townsend and Dr. Robert Buche for their critical comments and suggestions.

I have benefitted immensely from discussions with Dr. Anand Konanur, who served as a sounding board for my nascent ideas. I thank Ajit Rajagoplan with whom I had opportunity to collaborate on several projects. I would also like to acknowledge my colleagues: Dr. Vinit Singh, Dr. Stefan Schmidt, Carlos Cela, Randall Barlow, Ajeet, Sundar Srinivas, Amit Qusba, Nitin Qwatra and Zhengxin Tong for their constant support and encouragement. Several thought-provoking discussions of both technical and philosophical nature have been instrumental in making my graduate study a very remarkable one.

I have drawn much inspiration and support from my family. I have received immeasurable joy and love from my younger siblings, Vikas and Shilpi. My parent's unflinching support has inculcated in me steady confidence and determination. Their ceaseless prayers and blessings have been with me throughout my life. I dedicate my work to them.

TABLE OF CONTENTS

LIST OF TABLES

LIST OF FIGURES

Chapter 1

Introduction

Antenna design is as much an art as it is science. Even though several computation techniques are available today that can analyze any given antenna structure, fundamental understanding of electromagnetic theory is still indispensable for good antenna design. Based on one such fundamental insight, Andrews et al [1] proposed the concept of using six electromagnetic states of polarization (three electric and three magnetic) in an antenna system. These antennas are known as vector antennas or multi-polarized antennas. Their work spawned plethora of research on vector antennas to correctly assess the benefits they can provide in wireless communication systems.

The aim of the present work is to investigate these vector antennas and their applications. In particular, we study the impact of vector antennas when used in multiple-input multiple-output (MIMO) wireless communication systems and frequency selective surfaces (FSSs). Both these systems are formed from antenna arrays. The next section describes MIMO systems in detail. We then discuss FSSs in section 1.2. In section 1.3, we introduce the concept of vector antennas. Finally, we give a summary of the contributions of the present work in section 1.4.

1.1 MIMO Communication Systems

MIMO communication systems employ multiple antennas at the transmitter as well as the receiver, thus providing substantial increase in channel capacity in a rich scattering multi-path environment as compared to a single-input single-output (SISO) antenna systems. Figure 1.1 illustrates a MIMO communication system. The presence of scatterers

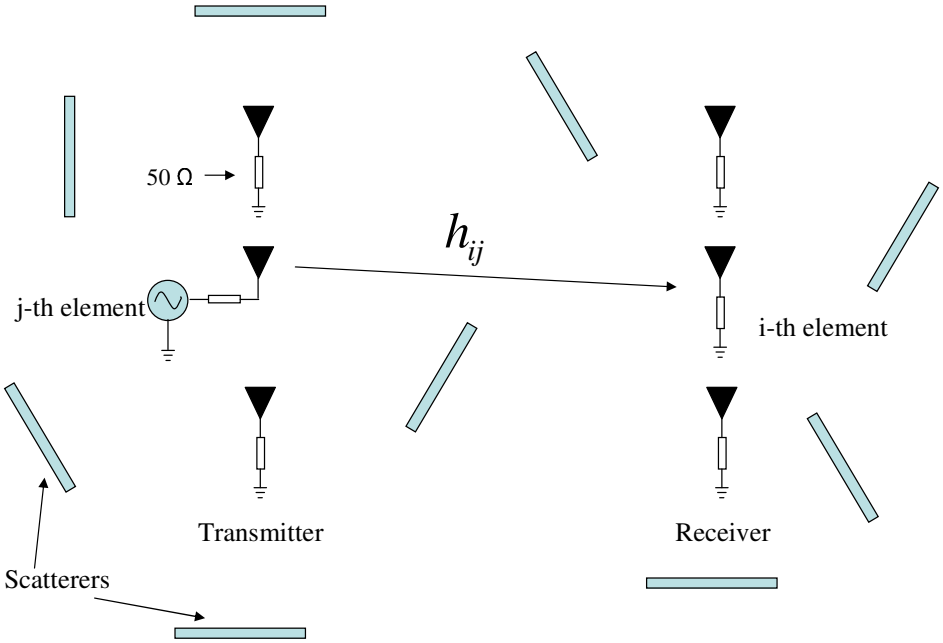

Figure 1.1: A MIMO Communication System

causes the transmitted signal to undergo multipath fading. If the delay between the signals reaching the receiver is small compared to the symbol time, then the channel is said to be frequency non-selective [2]. This occurs commonly in indoor wireless channels, where all the scatterers are located close to each other. Let h_{ij} denote the fading channel coefficient between j-th transmitter and the i-th receiver element. Then the $M \times 1$ vector of received signals can be compactly expressed with the following matrix equation

$$\mathbf{r} = \sqrt{\frac{\rho}{N}}\mathbf{H}\mathbf{x} + \mathbf{n} \tag{1.1}$$

where ρ is the signal-to-noise ration (SNR) per receive antenna, $\mathbf{H} = (h_{ij})$ is the $M \times N$ matrix of channel coefficients, $\mathbf{x}$ is the $N \times 1$ vector of transmitted signals and $\mathbf{n}$ is the additive receiver noise. It is a common assumption that the transmitted signals undergo Rayleigh fading and get corrupted by complex additive white gaussian noise (CAWGN).

The pioneering work of Foschini and Gans [3] and Telatar [4] showed that under suitable conditions the ergodic capacity of a communication system with N transmitters and M receivers is $\min(M, N)$ times the ergodic capacity of a single-input single-output system. Most conventional MIMO systems use spatial diversity by placing antennas three to ten wavelengths apart, thus achieving decorrelation of fading path gains which results in increased channel capacity.

Increased capacity can also be obtained by exploiting polarization and pattern diversity. Dual-polarized antennas have been used quite effectively for communication purposes. Andrews *et al* [1] suggested that the use of three orthogonally-polarized antennas (tripole) can provide a three-fold increase in capacity as compared to uni-polarized antennas. These antennas are capable of sensing more than one component of the electromagnetic field and are therefore referred to as vector antennas.

1.2 Frequency Selective Surfaces

In this section, frequency selective surfaces (FSSs) and their characteristics are introduced. Then the application of vector antennas in these surfaces is discussed.

FSSs are essentially periodic array structures, often in the form of printed structures on a substrate or apertures in a conducting plane. Figure 1.2 illustrates a typical FSS formed by arranging a unit element in two-dimensional array with inter-element spacings d_x and d_z along x- and z-axis, respectively. When an electromagnetic wave with strength

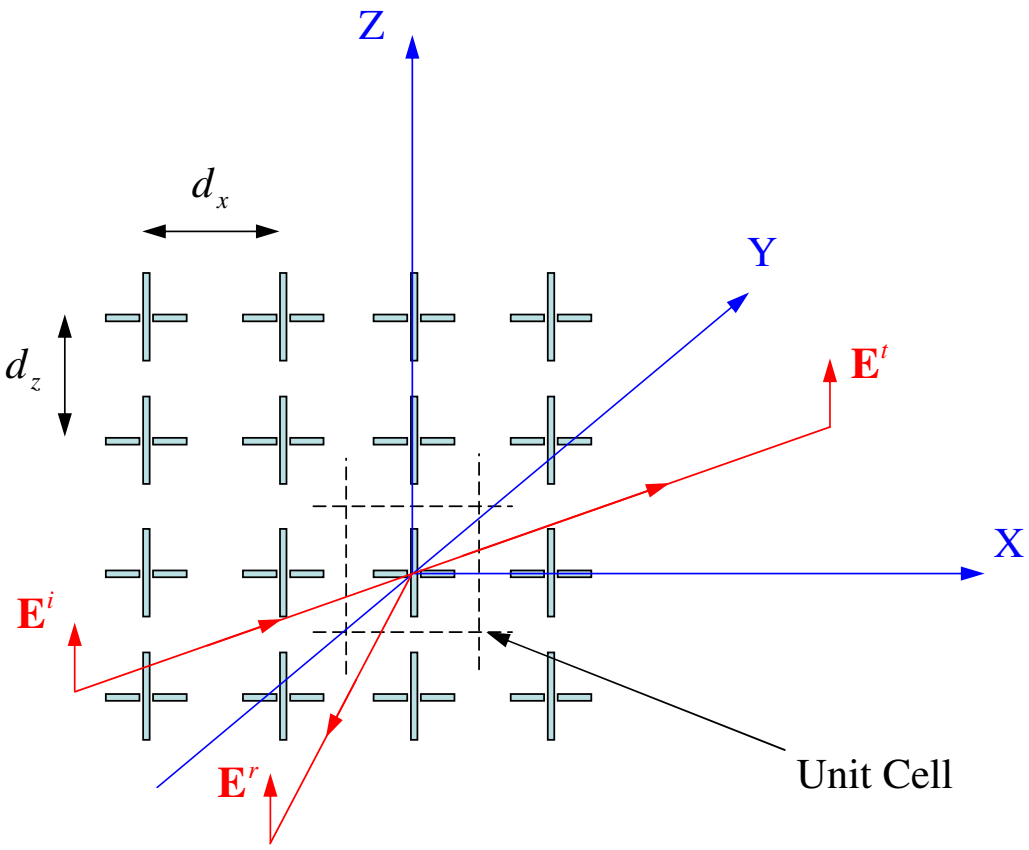

Figure 1.2: A Frequency Selective Surface

$\mathbf{E}^i$ is incident on the FSS, a part of it is reflected (with strength $\mathbf{E}^r$) and another part is transmitted (with strength $\mathbf{E}^t$). It is customary to define the reflection coefficient as

$$\Gamma = \frac{|\mathbf{E}^r|}{|\mathbf{E}^i|} \tag{1.2}$$

and the transmission coefficient as

$$T = \frac{|\mathbf{E}^t|}{|\mathbf{E}^i|}. \tag{1.3}$$

These surfaces behave as filters for incident electromagnetic waves based on frequency, polarization and angle of incidence of incident field. In other words, $\Gamma(f)$ and $T(f)$ are functions of the frequency of the incident field. Depending on the type and size of the elements as well as their spacing, certain frequencies are strongly reflected while others are strongly transmitted as illustrated in Figure 1.3. The resonant frequency, f_r, depends on the individual element of the unit cell that is repeated to produce the FSS. The bandwidth $(f_2 - f_1)$ of the surface depends on the type of element as well as the spacing between them. In fact, for a relatively large spacing the reflection coefficient response is narrowband and there is considerable variation in the backscattered response with the angle of incidence. If instead, the inter-element spacing is reduced together, the variation of the reflection coefficient with angle of incidence is lesser. In this case, however, the backscattered response is relatively broadband. The unit element can be categorized into four groups:- (i) center-connected or N-poles, (ii) loop types, (iii) solid interior or plate types and (iv) combinations of the above groups. An exhaustive survey of the types of unit element and their frequency response is available in [5, 6].

The goal of current research is to design FSSs on fabric such that the reflected signal has a distinguishing feature or 'signature'. This signature could be in the form of a specific frequency response or polarization of the reflected signal. Since individual components of the vector antenna interact with different components of the electromagnetic field, vector antennas can be used in FSSs. To illustrate this point, consider an element which consists of two crossed dipoles, one that is open and the other short. If the incident field has components along both the dipoles the reflected field will contain component only along the shorted dipole. This polarization information acts as a 'signature'.

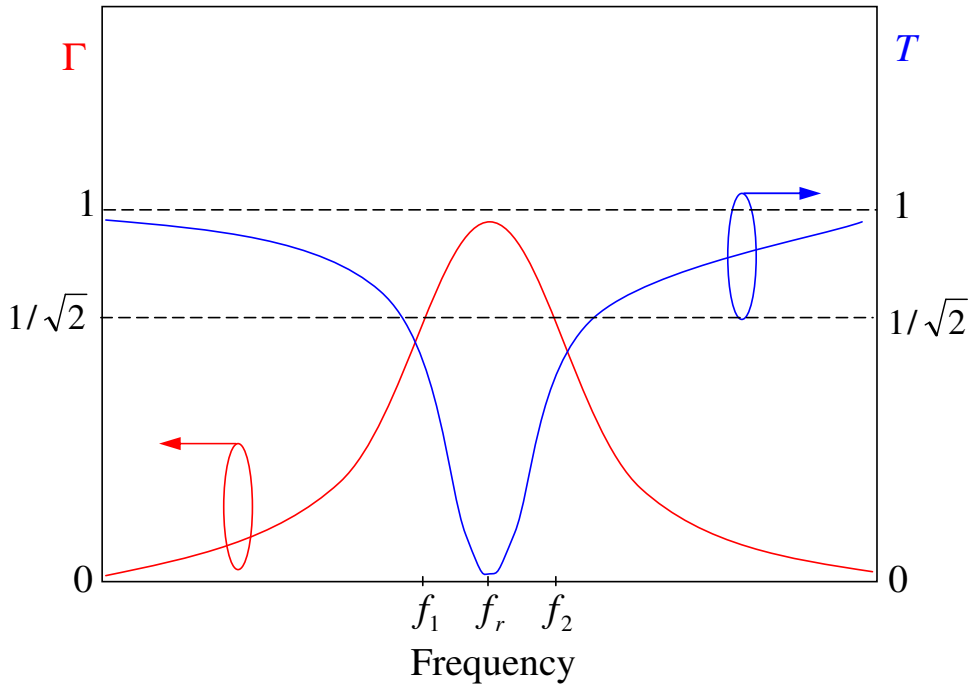

Figure 1.3: Illustration of reflection and transmission coefficient for a frequency selective surface

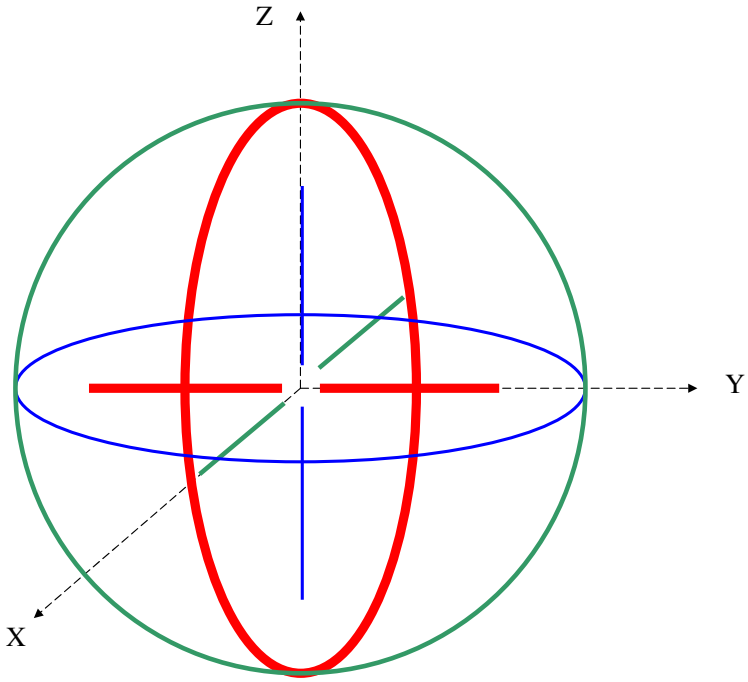

Figure 1.4: Vector Antenna

1.3 Vector Antenna

In this section a detailed description of vector antennas and their design considerations is given. A survey of previous research, analysis and fabricated prototype designs of these antennas is also provided.

1.3.1 Description

Conceptually, a vector antenna consists of multiple elements that can sense different components of the electromagnetic field. In its simplest form, three dipoles and three loops can be placed orthogonally to constitute a vector antenna as shown in the Figure 1.4. This configuration, theoretically, should sense all the components of both the electric and magnetic fields.

1.3.2 Design considerations

MIMO vector antennas have certain design considerations in addition to the design criterion for general antennas. In this subsection these design considerations are described through a set of metrics.

1. Reflection Coefficient

   The reflection coefficient (Γ) is defined as the ratio of the signal being reflected from the antenna to the signal being fed to the antenna. The magnitude of reflection coefficient is called the return loss and it is customary to represent it in decibels ($20\log_{10}(|\Gamma|)$). $\|\Gamma|^2$ is a measure of the power that is reflected back from the antenna and hence unusable. A low (typically less than -10 dB) value of return loss is desirable.

2. Mutual Coupling

   Mutual coupling refers to the phenomenon of a voltage or current signal being induced at one antenna due to a signal source at another antenna. This is especially important in the case of vector antennas in which individual elements are closely located and hence mutual coupling is no longer negligible. Research is ongoing to assess the impact of mutual coupling on MIMO antenna performance.

3. Radiation Efficiency

   The radiation efficiency is the ratio of power radiated by the antenna to the power fed to the antenna. The return loss, mutual coupling and ohmic losses in the antenna contribute to the reduction in radiation efficiency.

4. Radiation Pattern

   The radiation pattern is a description of the power radiated by the antenna as a function of angular coordinates. Certain antennas have highly directive patterns to increase signal-to-noise ratio (SNR) towards the receiving antennas and reduce interference for other antennas. Other antennas have omni-directional patterns for broadcast applications. The radiation pattern is very important for MIMO vector antennas because the antenna elements are placed very close together. Therefore their radiation patterns in isolation are modified due to the presence of other elements.

1.3.3 Analysis

Much research has been done to analyze and understand the benefits of vector antennas. Andrews *et al* [1] proposed that vector antenna can provide a six-fold increase in capacity as compared to uni-polarized antenna because of the existence of six independent (three electric and three magnetic) field components in the presence of multi-path. They simulated a vector antenna in a transceiver configuration with two reflecting surfaces and obtained 6 independent channels (non-zero eigenvalues of the channel).

Marzetta [7] analyzed the case of two-dimensional arrays of vector antennas and suggested that they behave differently from single vector antennas. Using plane-wave spectral decomposition he deduced that two-dimensional arrays of vector antennas can offer only a four-fold increase in capacity as compared to arrays of uni-polarized antennas. In his view, using three-dimensional arrays or using element spacing less than half-wavelength can produce only a logarithmic increase in capacity.

Poon *et al* [8] used a decomposition similar to the singular-value decomposition of the Green's function kernel to conclude that the increase in the number of degrees of freedom due to tri-polarization in arrays is two-fold as compared to arrays of uni-polarized antennas. Therefore, in the high SNR regime there can be only two-fold increase in capacity due to polarization.

Vector antennas can also perform better electromagnetic source localization than uni-polarized antennas as shown by Nehorai *et al* [9] since these antennas can use all the available information in the different components of electromagnetic field.

1.3.4 Fabricated designs

Several prototypes of vector antennas have been fabricated and tested. Andrews *et al* [1] used three standard sleeves arranged orthogonally to form a tripole. Stancil *et al* [10] designed a two-element vector antenna using a conventional half-wavelength dipole and a magnetic dipole (Kandoian loop) for their experiments. Konanur *et al* [11] designed a three-element (two half-wavelength dipoles and a center-fed loop) planar antenna and a four-element (three half-wavelength dipoles and a center-fed loop) vector antenna. Rajagopalan *et al* [12] recently published a three-element (two bowtie and a loop) ultrawideband vector antenna.

1.4 Overview of Contributions

In this dissertation, we use theoretical, simulation and measurement techniques to assess the performance improvements that vector antennas can provide in multiple antenna systems.

In chapter 2, we analyze a linear array of vector antennas using signal-space concepts. More specifically, it has been shown that the degrees of freedom of the fields produced by a linear array of tri-polarized antennas is three times that of uni-polarized antennas. This increase in the degrees of freedom implies the possibility of a three-fold increase in channel capacity at high SNR.

Next, we focus our attention on practical aspects of antenna design. In chapter 3, we have used method of moments to simulate and optimize antenna structures to meet the design guidelines prescribed in section 1.3.2. Based on these designs, narrowband and broadband tri-polarized antennas have been fabricated. We then illustrate an experimental setup that can be used to perform MIMO channel measurements in a laboratory setting. The measurement setup consists of a network analyzer, which is used to determine the channel path gains by measuring the S_{21} parameters between every pair of transmit and receive antennas. The scatterers are placed according to the two-dimensional model proposed in [13].

To assess the improvement in spectral efficiency due to polarization, we calculate channel capacity of MIMO systems using the fabricated vector antennas in chapter 4. As a reference, capacity of MIMO systems using infinitesimally small tri-polarized antennas has also been evaluated. Detailed three-dimensional channel models [14, 15] have been used for simulating arrays of different length. Both the simulation and measurement results show that a three-fold increase in capacity can be obtained using array of tri-polarized antennas as compared an equivalent array of uni-polarized antennas.

Multiple antennas are also used in frequency selective surfaces in two-dimensional array configuration. In chapter 5, we study the improvement in the reflected energy that vector antennas can provide as compared to conventional uni-polarized antennas when integrated on FSS. For this purpose, we have fabricated and tested several prototypes of FSSs on fabric with vector antennas as unit elements. Our results show that the use of vector antennas increases the reflected mean-signal-energy and also makes the design more robust to misalignment.

Chapter 2

Degrees of Freedom

2.1 Introduction

In this chapter, we analyze the degrees of freedom of linear arrays of tri-polarized antenna systems. The degrees of freedom of fields radiated from uni-polarized antenna systems for arbitrary geometries have been calculated by Bucci et al [16] and Poon et al [8]. They have considered antenna systems as continuous sources, i.e., every point of the antenna system can be excited by arbitrary current density. This assumption leads to two drawbacks. Firstly, it allows for the possibility of infinite degrees of freedom. Secondly, the current density on any practical antenna element is determined by its geometry and cannot be arbitrarily adjusted. In the present work, we circumvent the first problem by considering that the antenna system has only finite number of antenna elements, each of which has its own current excitation. This automatically limits the degrees of freedom of the system to finite values. In addition, the current profile on each antenna element is assumed to be determined by its geometry.

In previous research work, the degrees of freedom of polarized antenna systems has been analyzed only heuristically [8, 7]. Our analysis shows a three-fold increase in degrees of freedom of an array of tri-polarized antennas compared to an equivalent array of uni-polarized antennas. More specifically, this finding holds true for three different types of antenna elements:- infinitesimally small dipoles, finite length dipoles and long wire traveling wave antennas. This three-fold increase in degrees of freedom is a necessary condition to obtain a corresponding three-fold increase in channel capacity at high signal-to-noise ratio (SNR).

In the subsequent sections, we consider the electric field generated by a linear array of tri-polarized antennas on the surface of a large surrounding sphere. Our aim is to demonstrate that the number of degrees of freedom (DoF) available in this system is exactly three times the number available in a corresponding linear array of uni-polarized antennas. Thus, the use of tri-polarized antennas increases the number of available signaling dimensions by a factor of three relative to an array of uni-polarized antennas.

In the following analysis we use vector-phasor notation $\mathbf{U}(\mathbf{r})$ to represent the time-harmonic function

$$\mathbf{U}(\mathbf{r},t) = Re\left[\mathbf{U}(\mathbf{r})e^{i\omega t}\right] \tag{2.1}$$

of position $\mathbf{r}$, center angular frequency ω and time t. The magnitude and the unit vector corresponding to any vector $\mathbf{u}$ are denoted by u and $\hat{\mathbf{u}} = \mathbf{u}/u$, respectively. We first consider the case of antenna elements that are infinitesimally small to describe the concept of degrees of freedom. The tools developed in section 2.2 serve as an aid to analyze the more practical finite length antenna elements, namely dipoles (section 2.3) and long-wire antennas (section 2.4).

2.2 Linear Array of Infinitesimally Small Antennas

We model the array as a current source of length $2L$ oriented along the z-axis and centered at the origin, as shown in Figure 2.1. If the array consists of N infinitesimal tripoles located at $\{\mathbf{r}' = z'_s\hat{\mathbf{z}} : z'_s \in [-L, L] \text{ for } s = 1, 2, \ldots, N\}$, where $\hat{\mathbf{z}}$ is the unit vector along the z-axis, then the current source distribution can be expressed as

$$\mathbf{J}(\mathbf{r}') = \sum_{s=1}^{N} \mathbf{J}_s \delta_{z'-z'_s} \tag{2.2}$$

where $\mathbf{J}_s = [J_{sx}, J_{sy}, J_{sz}]^T \in \mathbb{C}^3$ and $\delta_{\cdot}$ is the Dirac function.

The rectangular components of the electric field in the far-field region (in air) due to this current source are given by [8]

$$\mathbf{E}(\mathbf{r}) = \int_{V'} \mathbf{G}(\mathbf{r},\mathbf{r}')\mathbf{J}(\mathbf{r}')dv' \tag{2.3}$$

$$\mathbf{G}(\mathbf{r},\mathbf{r}') = \frac{i\omega\mu}{4\pi}\frac{e^{ikr}}{r}(\mathbf{I} - \hat{\mathbf{r}}\hat{\mathbf{r}}^T)e^{-ik\hat{\mathbf{r}}^T\mathbf{r}'} \tag{2.4}$$

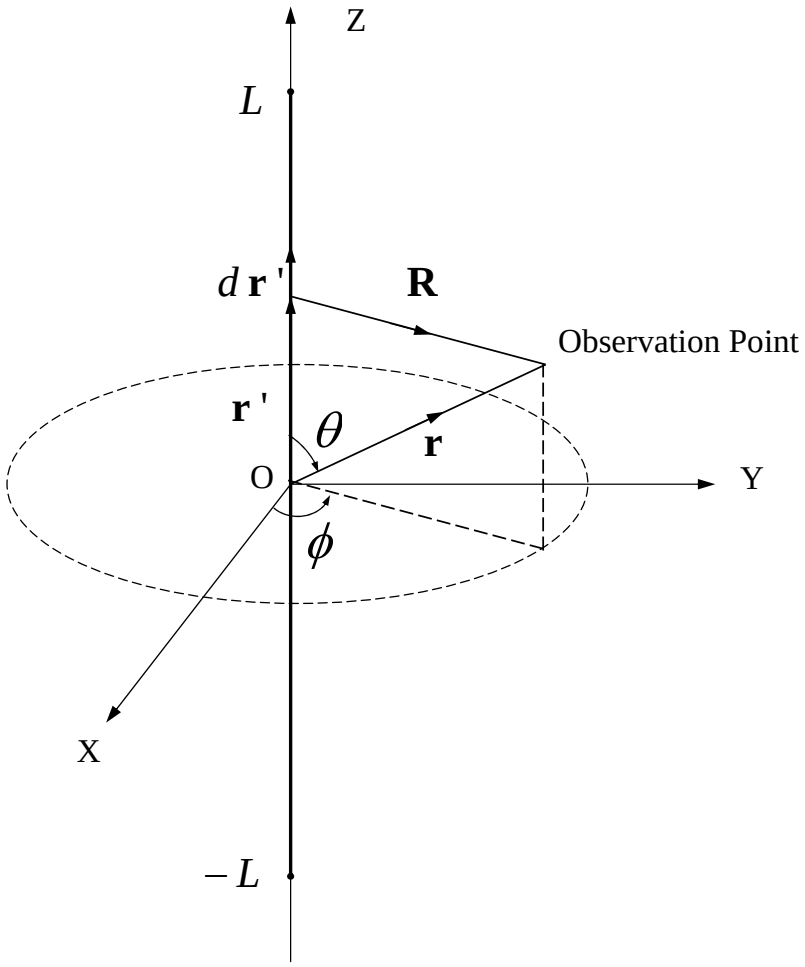

Figure 2.1: Geometry of the current source and the coordinate system

where $\mathbf{G}(\mathbf{r}, \mathbf{r}')$ is the Green's function, μ is the magnetic permeability of air, c is the speed of light, $k = \omega/c$ is the angular wavenumber and $\hat{\mathbf{r}} = [\sin\theta\cos\phi \quad \sin\theta\sin\phi \quad \cos\theta]^T$.

A simpler formulation can be obtained by expressing the electric field in spherical components. Using the transformation matrix $\mathbf{C}$ [17, eq. VII-12a] the spherical components can be written as

$$\begin{bmatrix} E_r \\ E_\theta \\ E_\phi \end{bmatrix} = \underbrace{\begin{bmatrix} \sin\theta\cos\phi & \sin\theta\sin\phi & \cos\theta \\ \cos\theta\cos\phi & \cos\theta\sin\phi & -\sin\theta \\ -\sin\phi & \cos\phi & 0 \end{bmatrix}}_{\mathbf{C}} \begin{bmatrix} E_x \\ E_y \\ E_z \end{bmatrix}. \tag{2.5}$$

We use the following simplification when substituting (2.3) in (2.5)

$$\mathbf{C}(\mathbf{I} - \hat{\mathbf{r}}\hat{\mathbf{r}}^T) = \begin{bmatrix} 0 & 0 & 0 \\ \cos\theta\cos\phi & \cos\theta\sin\phi & -\sin\theta \\ -\sin\phi & \cos\phi & 0 \end{bmatrix}. \tag{2.6}$$

This field is observed on the surface of a sphere of radius $r \gg L$ centered at the origin. Since r is constant on this sphere, the explicit dependence of the field on r can be dropped. Further, since the radial component vanishes in the far-field (which is evident from (2.6)), we only consider the θ and ϕ components of the electric field in spherical coordinates as

$$\mathbf{E}(\theta, \phi) = [E_\theta(\theta, \phi) \; E_\phi(\theta, \phi)]^T = \mathbf{N}(\theta, \phi)\mathbf{A}(\theta, \phi) \tag{2.7}$$

where

$$\mathbf{N}(\theta, \phi) = i\omega \begin{bmatrix} \cos\theta\cos\phi & \cos\theta\sin\phi & -\sin\theta \\ -\sin\phi & \cos\phi & 0 \end{bmatrix} \tag{2.8}$$

and $\mathbf{A}(\theta, \phi)$ is the vector potential

$$\mathbf{A}(\theta, \phi) = \frac{\mu}{4\pi}\frac{e^{ikr}}{r}\int_{V'} e^{-ik\hat{\mathbf{r}}^T\mathbf{r}'}\mathbf{J}(\mathbf{r}')dv' \; . \tag{2.9}$$

Substituting (2.2) into (2.9), we obtain

$$\mathbf{A}(\theta, \phi) = \mathbf{D}(\theta) = \sum_{s=1}^{N} \mathbf{J}_s a_s(\theta) \tag{2.10}$$

where $a_s(\theta) = \frac{\mu}{4\pi}\frac{e^{ikr}}{r}e^{-ikz_s'\cos\theta}, 1 \le s \le N$. The collection of all fields $\mathbf{E}(\theta, \phi)$ that can be produced by varying $\mathbf{J}_1, \ldots, \mathbf{J}_N$ clearly constitutes a complex linear space $\mathcal{L}_E$ of functions

over $0 \leq \theta < \pi$, $-\pi \leq \phi < \pi$. We now show that the dimension of this space, which is called the *degrees of freedom*, is exactly three times the dimension of a corresponding uni-polarized system. To this end, we first consider the complex linear space $\mathcal{L}_D$ of all functions $\mathbf{D}(\theta)$ produced by varying $\mathbf{J}_1, \ldots, \mathbf{J}_N$ (this is the same linear space $\mathcal{L}_A$ of all vector potentials $\mathbf{A}(\theta, \phi)$). Note that $a_s(\theta), 1 \leq s \leq N$ are continuous scalar functions of θ. Thus $\mathbf{D}(\theta)$ must also be continuous. For uni-polarized antenna systems, the vectors $\mathbf{J}_1, \ldots, \mathbf{J}_N$ lie in a one-dimensional subspace. Without loss of generality, suppose these vectors are aligned with the x-axis, $\mathbf{J}_s = [J_{x,s},\ 0,\ 0]^T$, $1 \leq s \leq N$. In this case, we have $\mathbf{D}(\theta) = [D_x(\theta),\ 0,\ 0]^T$, where $D_x(\theta)$ is any element in the complex linear space $\mathcal{L}$ spanned by $a_1(\theta), \ldots, a_N(\theta)$. If the dimension of $\mathcal{L}$ is denoted by $d \leq N$, then for uni-polarized antennas $\dim(\mathcal{L}_A) = \dim(\mathcal{L}_{\mathrm{D}}) = \mathrm{d}$.

In the tri-polarized case, the components of $\mathbf{J}_1, \ldots, \mathbf{J}_N$ can be selected independently, so the three components of $\mathbf{D}(\theta)$ are arbitrary elements of $\mathcal{L}$. It follows that $\mathcal{L}_D = \mathcal{L}^3$ and $\dim(\mathcal{L}_D) = 3d$. To show that $\dim(\mathcal{L}_E)$ for tri-polarized antenna systems is three times as large as that for uni-polarized antenna systems, it only remains to show $\dim(\mathcal{L}_E) = \dim(\mathcal{L}_D)$ in both cases. From (2.7), we see that a set of functions that span $\mathcal{L}_E$ can by obtained from any set of functions that span $\mathcal{L}_D$ by multiplying by $\mathbf{N}(\theta, \phi)$; hence $\dim(\mathcal{L}_E) \leq \dim(\mathcal{L}_D)$. To show $\dim(\mathcal{L}_E) = \dim(\mathcal{L}_D)$, we need only to show that the mapping $\mathbf{D}(\theta) \rightarrow \mathbf{N}(\theta, \phi)\mathbf{D}(\theta)$ is invertible. From (2.7) and (2.10) observe

$$\begin{aligned} D_x(\theta)\cos\theta &= 2\int_{-\pi}^{\pi} \cos\phi\ E_\theta(\theta,\phi)\ d\phi \\ D_y(\theta)\cos\theta &= 2\int_{-\pi}^{\pi} \sin\phi\ E_\theta(\theta,\phi)\ d\phi \\ D_z(\theta)\sin\theta &= -\int_{-\pi}^{\pi} E_\theta(\theta,\phi)\ d\phi \end{aligned} \tag{2.11}$$

Thus $\mathbf{D}(\theta)$ can be recovered from $E_\theta(\theta, \phi)$ for $\theta \neq 0, \pi/2, \pi, 3\pi/2$ and the remaining values can be obtained from continuity of $\mathbf{D}(\theta)$. We therefore conclude $\mathbf{D}(\theta) \rightarrow \mathbf{E}(\theta, \phi) = \mathbf{N}(\theta, \phi)\mathbf{D}(\theta)$ is invertible and $\dim(\mathcal{L}_E) = \dim(\mathcal{L}_D) = 3d$.

Thus we have established that the degrees of freedom for the electric field due to tri-polarized antennas is three times that due to uni-polarized antenna systems in the case of infinitesimally small elements. From (2.11), we further observe that it is not necessary to

observe the entire electric field to obtain all the $3d$ degrees of freedom. Observing $E_\theta(\theta, \phi)$ alone suffices to provide all $3d$ degrees of freedom.

2.3 Linear Array of Finite Length Antennas

We now consider the more practical case of antenna elements with finite length. Let the current distribution on each antenna element be given by function $f(\cdot)$, then the current source distribution in (2.2) has to be modified to

$$\mathbf{J}(\mathbf{r}') = \sum_{s=1}^{N} \mathbf{F}(\mathbf{r}', z_s')\mathbf{J}_s \tag{2.12}$$

where

$$\mathbf{F}(\mathbf{r}', z_s') = \begin{bmatrix} f(x')\delta_{y',z'-z_s'} & 0 & 0 \\ 0 & f(y')\delta_{x',z'-z_s'} & 0 \\ 0 & 0 & f(z'-z_s')\delta_{x',y'} \end{bmatrix}. \tag{2.13}$$

Substituting (2.13) in (2.9) and solving the integration

$$\begin{aligned} \mathbf{A}(\theta, \phi) &= \mathbf{B}(\theta, \phi) \sum_{s=1}^{N} a_s(\theta)\mathbf{J}_s & (2.14) \\ &= \mathbf{B}(\theta, \phi)\mathbf{D}(\theta) & (2.15) \end{aligned}$$

where

$$\begin{aligned} \mathbf{B}(\theta, \phi) &= \begin{bmatrix} B(x/r) & 0 & 0 \\ 0 & B(y/r) & 0 \\ 0 & 0 & B(z/r) \end{bmatrix} & (2.16) \\ &= \begin{bmatrix} B_x(\theta, \phi) & 0 & 0 \\ 0 & B_y(\theta, \phi) & 0 \\ 0 & 0 & B_z(\theta, \phi) \end{bmatrix} & (2.17) \end{aligned}$$

and

$$B(u) = \int_l e^{-ikwu} f(w) dw. \tag{2.18}$$

$B(u)$ is responsible for the different radiation patterns that the antenna elements have due to their current distributions. The expression in (2.15) is similar to section 2.2 but the vector potential has been modified by $\mathbf{B}(\theta, \phi)$ to include the effect of current distribution.

$$\mathbf{J}(z') = \sin\left[k\left(\frac{l}{2} - |z'|\right)\right] J_0 \hat{\mathbf{z}} \quad \text{for} \quad |z'| \le \frac{l}{2}$$

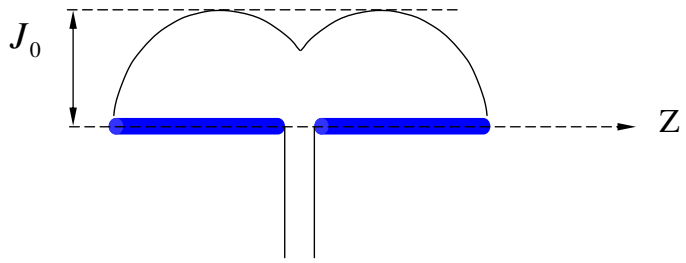

Figure 2.2: Finite length dipole antenna

The electric field, $\mathbf{E}(\theta, \phi) = \mathbf{N}(\theta, \phi)\mathbf{A}(\theta, \phi)$ still has the same expression as in (2.7). For a z-directed thin dipole of length l we have [17] (see Figure 2.2),

$$f(w) = \sin\left[k\left(\frac{l}{2} - |w|\right)\right], |w| \le \frac{l}{2} \tag{2.19}$$

and

$$E_\theta = i\frac{\omega\mu}{k}\frac{1}{2\pi}\frac{e^{ikr}}{r}\left[\frac{\cos(\frac{kl}{2}\cos\theta) - \cos(\frac{kl}{2})}{\sin\theta}\right]. \tag{2.20}$$

Substituting (2.19) in (2.18) we obtain

$$B(u) = -\frac{2}{k}\left[\frac{\cos(\frac{kl}{2}u) - \cos(\frac{kl}{2})}{1 - u^2}\right]. \tag{2.21}$$

Using (2.17) with the above equation and recalling $[x, y, z] = [r\sin\theta\cos\phi, r\sin\theta\sin\phi, r\cos\theta]$, we can write

$$B_x(\theta, \phi) = -\frac{2}{k}\left[\frac{\cos(\frac{kl}{2}\sin\theta\cos\phi) - \cos(\frac{kl}{2})}{1 - (\sin\theta\cos\phi)^2}\right] \tag{2.22}$$

$$B_y(\theta, \phi) = -\frac{2}{k}\left[\frac{\cos(\frac{kl}{2}\sin\theta\sin\phi) - \cos(\frac{kl}{2})}{1 - (\sin\theta\sin\phi)^2}\right] \tag{2.23}$$

$$B_z(\theta, \phi) = -\frac{2}{k}\left[\frac{\cos(\frac{kl}{2}\cos\theta) - \cos(\frac{kl}{2})}{\sin^2\theta}\right] \tag{2.24}$$

(2.25)

We now proceed to show that the mapping $\mathbf{D}(\theta) \rightarrow \mathbf{E}(\theta,\phi) = \mathbf{N}(\theta,\phi)\mathbf{B}(\theta,\phi)\mathbf{D}(\theta)$ is invertible for dipole antennas of any length. It is helpful to write (2.7) in expanded form using (2.15)

$$\begin{aligned} E_\theta(\theta,\phi) =& i\omega[\cos\theta\cos\phi B_x(\theta,\phi)D_x(\theta) \\ &+ \cos\theta\sin\phi B_y(\theta,\phi)D_y(\theta) - \sin\theta B_z(\theta,\phi)D_z(\theta)] \\ E_\phi(\theta,\phi) =& i\omega[-\sin\phi B_x(\theta,\phi)D_x(\theta) + \cos\phi B_y(\theta,\phi)D_y(\theta)] \end{aligned} \tag{2.26}$$

Note that both B_x and B_y are even functions of ϕ. Thus $\mathbf{D}(\theta)$ can be obtained from $\mathbf{E}(\theta,\phi)$ by doing the following operations in succession

$$\begin{aligned} \int_{-\pi}^{\pi} \cos\phi E_\phi(\theta,\phi)B_y^*(\theta,\phi)d\phi &= i\omega D_y(\theta)\int_{-\pi}^{\pi}|B_y(\theta,\phi)|^2 \\ &\quad\times\cos^2\phi d\phi \\ i\omega B_x(\theta,\phi)D_x(\theta)\sin\phi &= -E_\phi(\theta,\phi) \\ &\quad + i\omega B_y(\theta,\phi)D_y(\theta)\cos\phi \\ -i\omega B_z(\theta,\phi)D_z(\theta)\sin\theta &= E_\theta(\theta,\phi) \\ &\quad - i\omega B_x(\theta,\phi)D_x(\theta)\cos\theta\cos\phi \\ &\quad - i\omega B_y(\theta,\phi)D_y(\theta)\cos\theta\sin\phi \end{aligned} \tag{2.27}$$

provided

(a) $\int_{-\pi}^{\pi}|B_y(\theta,\phi)|^2\cos^2\phi d\phi \neq 0 \Leftrightarrow B_y(\theta,\phi) \neq 0$ for all ϕ

(b) $B_x(\theta,\phi)\sin\phi \neq 0$ for all ϕ

(c) $B_z(\theta,\phi)D_z(\theta)\sin\theta \neq 0$

For z-directed dipoles, conditions (a) and (b) can possibly be violated at $\theta = 0$ and (c) when $\cos\theta = 1 - (n\lambda)/(l) \quad n = 0,1,2,\ldots$. Since these values of θ are isolated, $\mathbf{D}(\theta)$ can be obtained by continuity. Thus we have proved that the mapping $\mathbf{D}(\theta) \rightarrow \mathbf{N}(\theta,\phi)\mathbf{B}(\theta,\phi)\mathbf{D}(\theta)$ is invertible and $\dim(\mathcal{L}_E) = \dim(\mathcal{L}_D)$.

2.4 Linear Array of Traveling Wave Antennas

We now consider the long wire antenna element which is a type of traveling wave antenna. The current flows on a traveling wave antenna in the form of traveling waves as

$$\mathbf{J}(z') = e^{-(\alpha+ik)z'} J_0 \hat{\mathbf{z}} \quad \text{for} \quad 0 \le z' \le l$$

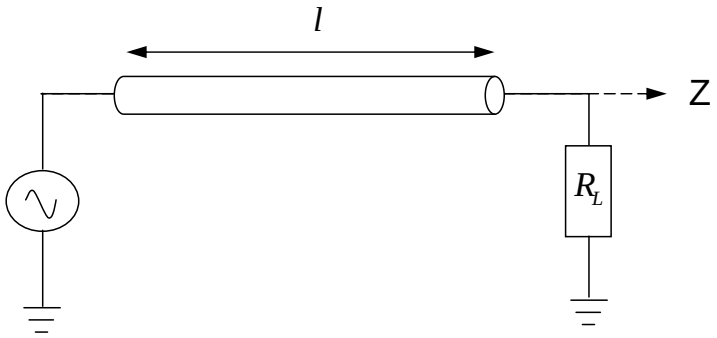

Figure 2.3: Long wire traveling wave antenna

compared to standing waves on resonant antenna like dipoles which we discussed in the previous section. Usually these antennas are broadband structures. A z-directed long wire traveling wave antenna element is shown in Figure 2.3. The current distribution on this element is given by [17]

$$f(w) = e^{-(\alpha+ik)w} \tag{2.28}$$

where k is the propagation constant of the traveling wave. As the wave travels, it loses energy which is accounted by the attenuation factor α. It is assumed that an ideal matched termination resistance R_L absorbs all the waves traveling in the positive z-direction and there are no reflections. The termination resistance should equal the value of the radiation resistance of the antenna [18, 19] (this is usually in the region of 200Ω to 300Ω). Substituting the current distribution in (2.18), we get

$$B(u) = \frac{1 - e^{-[\alpha+ik(1+u)]l}}{\alpha + ik(1+u)} \tag{2.29}$$

Using (2.17) and observing that $x = \sin\theta\cos\phi$, $y = \sin\theta\sin\phi$ and $z = \cos\theta$ we have

$$B_x(\theta,\phi) = \frac{1 - e^{-[\alpha+ik(1+\sin\theta\cos\phi)]l}}{\alpha + ik(1+\sin\theta\cos\phi)} \tag{2.30}$$

$$B_y(\theta,\phi) = \frac{1 - e^{-[\alpha+ik(1+\sin\theta\sin\phi)]l}}{\alpha + ik(1+\sin\theta\sin\phi)} \tag{2.31}$$

$$B_z(\theta,\phi) = \frac{1 - e^{-[\alpha+ik(1+\cos\theta)]l}}{\alpha + ik(1+\cos\theta)} \tag{2.32}$$

Again, $\mathbf{D}(\theta)$ can be obtained from $\mathbf{E}(\theta,\phi)$ by using (2.7) in conjunction with (2.15) and doing the following operations in succession

$$\begin{aligned} E_\phi(\theta,\frac{\pi}{2}) &= -i\omega B_x(\theta,\frac{\pi}{2})D_x(\theta) \\ E_\phi(\theta,0) &= i\omega B_y(\theta,0)D_y(\theta) \\ i\omega\sin\theta B_z(\theta,0)D_z(\theta) &= i\omega\cos\theta B_x(\theta,0)D_x(\theta) - E_\theta(\theta,0) \end{aligned} \tag{2.33}$$

provided

(a) $B_x(\theta,\frac{\pi}{2}) \neq 0$,

(b) $B_y(\theta,0) \neq 0$ and

(c) $\sin\theta B_z(\theta,0) \neq 0$.

Since $\alpha \neq 0$ conditions (a) and (b) cannot be violated. Condition (c) can be violated only at the isolated point $\theta = 0$ where $\mathbf{D}(\theta)$ can be obtained by continuity. Thus we have proved that the mapping $\mathbf{D}(\theta) \rightarrow \mathbf{N}(\theta,\phi)\mathbf{B}(\theta,\phi)\mathbf{D}(\theta)$ is invertible and $\dim(\mathcal{L}_E) = \dim(\mathcal{L}_D)$.

Chapter 3

Antenna Design and Experimental Setup

3.1 Introduction

The degrees of freedom analysis in chapter 2 assumed that the radiation patterns of antenna elements are ideal and that they radiate independently of each other. In a practical system, however, the radiation patterns of the antenna elements can become distorted and inter-element mutual coupling increases as they are brought closer. Therefore, in this chapter we present several antenna system designs and fabricated prototypes that account for these non-idealities. More specifically, sections 3.2 and 3.3 discuss the design and fabrication process of tri-polarized antenna systems with dipole and traveling wave antenna elements. We will also describe measurement techniques in section 3.4 that will help in assessing the performance benefits of tri-polarized antenna systems in chapter 4.

3.2 Design of Tripole

In this section we describe the design of a co-located tri-polarized antenna with dipole elements. A four-element polarized antenna with three orthogonal dipoles and a loop has been fabricated and studied in [20]. In that design, the dipoles had to be fed off-centered to accommodate all the four feed elements (SMA connectors) resulting in inter-element spacing. Reducing this spacing is important to ensure that any increase in capacity is due to polarization instead of spatial diversity. The design presented here aims to achieve

this by feeding the dipole through a co-planar strip (CPS). Figure 3.1 shows a schematic of the tripole arrangement of co-located printed dipoles, where each individual element is designed based on the idea proposed in [21].

The dipoles were fabricated on a substrate with relative dielectric permittivity of 2.6. The return loss and coupling for the design simulated with the commercial software Agilent ADS is compared with the results obtained using fabricated antennas in Figure 3.2. Further, the return loss and coupling for the designed tripole for all possible pairs are shown in figure 3.3. The return loss is below -10 dB and the coupling is below -20 dB in the frequency range 3.75 to 3.85 GHz in all cases and hence satisfactory for our purpose. While measuring the S-parameters between any pair of elements of a vector antenna, the other elements are always terminated in matched loads.

3.3 Design of Traveling Wave Antenna

In this section, the practical design of a traveling wave antenna is described. Figure 3.4(a) shows a long wire antenna that is terminated in a matched load R_L. As mentioned in section 2.4, the purpose of the termination resistor is to suppress any reflections which may result in standing waves. There are a couple of practical problems with this design. Firstly, it requires the ground plane to extend to one of the terminals of the resistor. The extended ground plane can cause high coupling between the elements when used in a tri-polarized setup. Secondly, it requires the availability of a broadband matched resistor that has negligible parasitics at high frequencies used for communication purposes (around 1-10 GHz). These resistors are quite costly and can increase the cost of the antenna.

Both the problems mentioned above can be avoided if the length of the antenna is made several wavelengths long as shown in Figure 3.4(b). In this case, the forward traveling wave attenuates due to radiation as well as losses before it reaches the end of the wire and therefore the resistor is not required. Even though the matched load is not required in this design, it becomes unwieldy in applications where space may be limited. An alternative is to use a meanderline antenna to compress the length in a small space as shown in Figure 3.4(c). Warnagiris et al [22] have used meanderline concept to design antennas at lower frequencies (30-60 MHz). Based on this design, Seong et al [23] fabricated a miniaturized dipole at 2.5 GHz and 5.25 GHz with meanderline for laptop computers. In both these designs, there exist current components that are not along z-axis. Therefore, the field produced by this

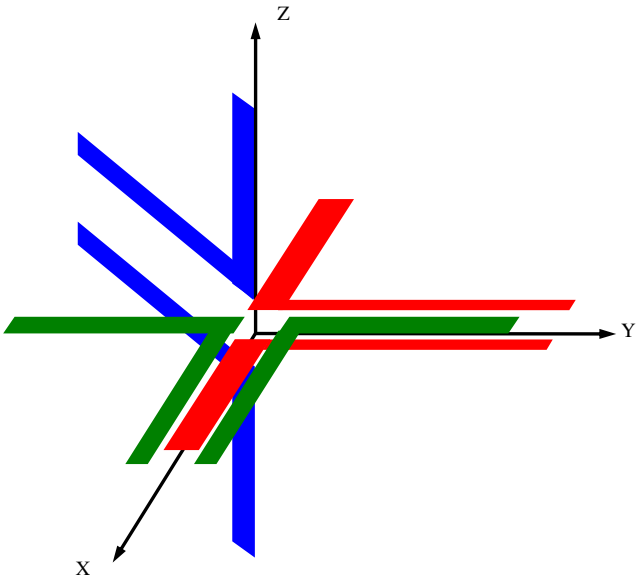

(a) Arrangement of dipoles to form a tripole antenna

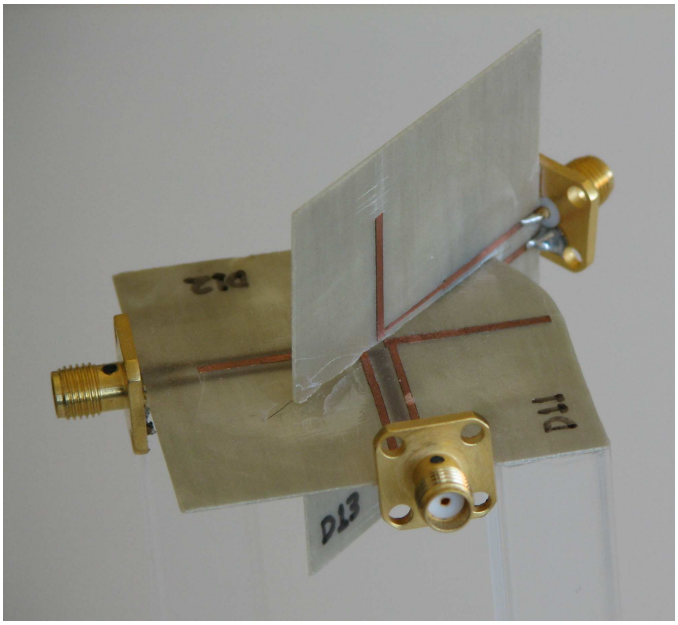

(b) Fabricated tripole

Figure 3.1: The Tri-polarized Antenna

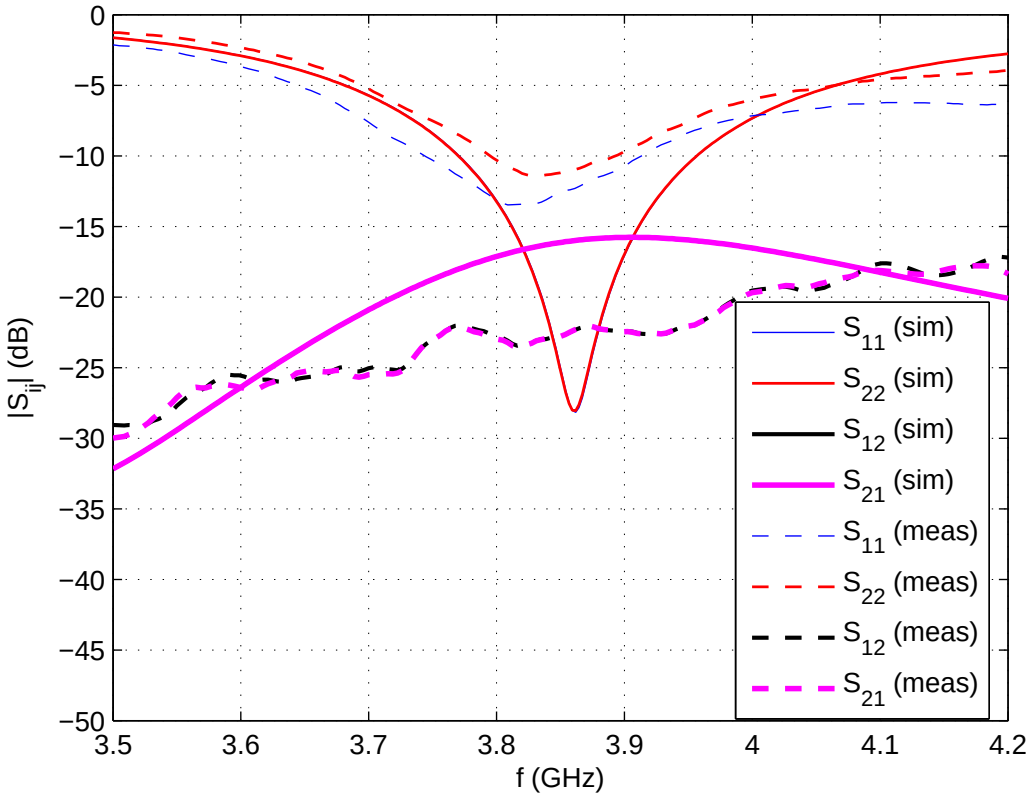

Figure 3.2: Comparison of simulated and measured return loss and coupling between elements of tripole antenna

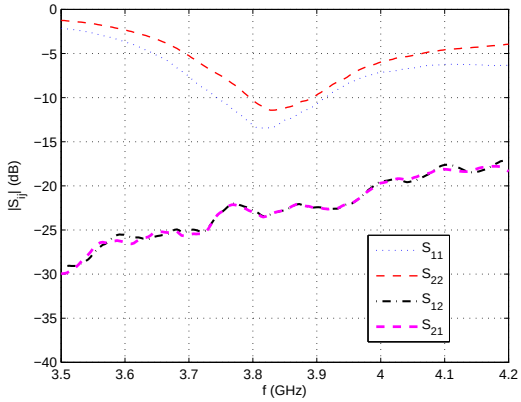

(a) x-directed and y-directed dipole

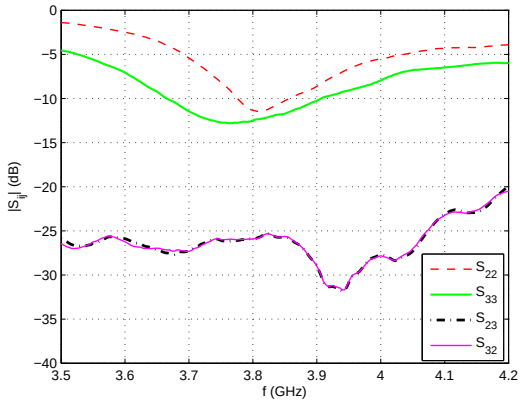

(b) y-directed and z-directed dipole

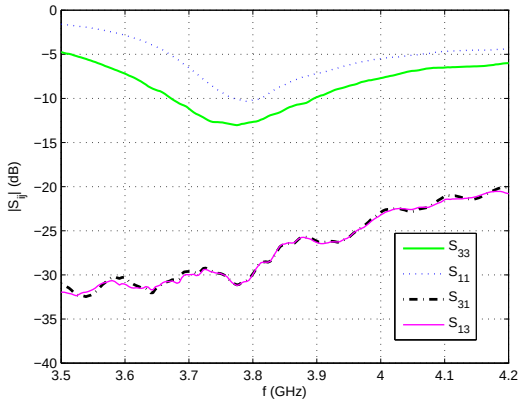

(c) z-directed and x-directed dipole

Figure 3.3: Pairwise return loss and coupling between elements of tripole antenna

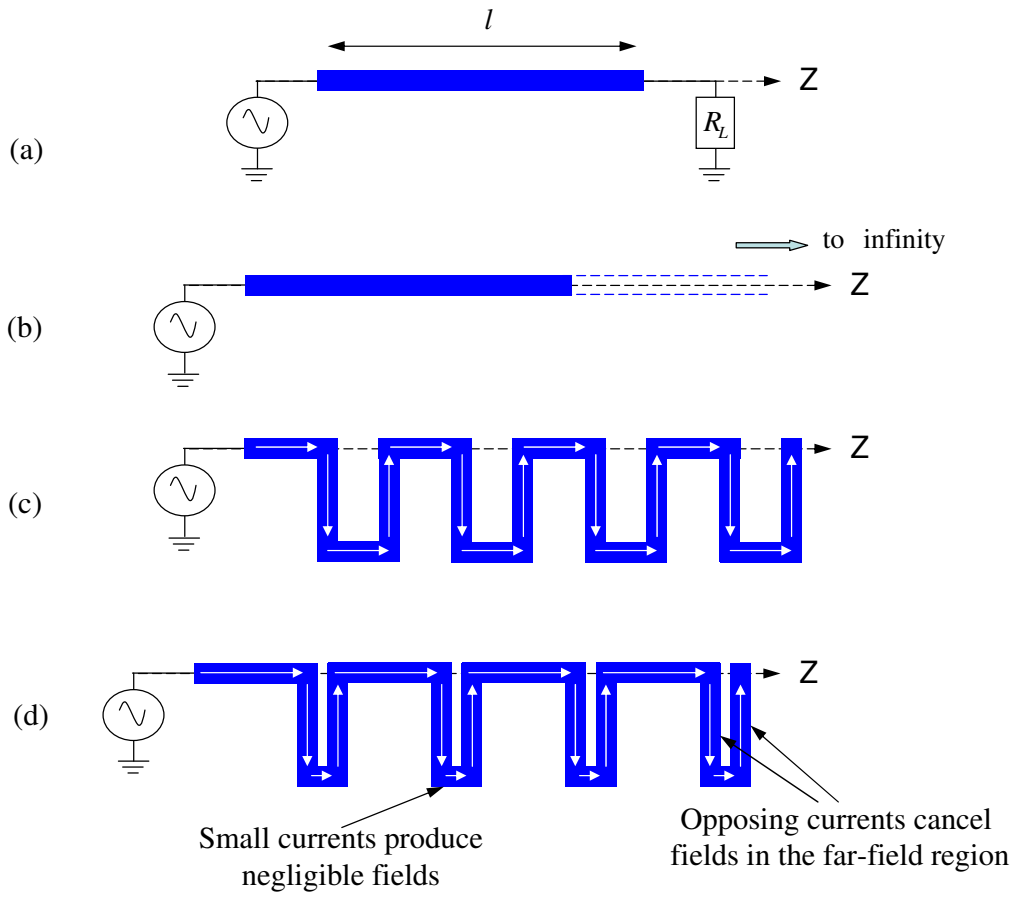

Figure 3.4: Meanderline traveling wave antenna concept

design will not coincide with that mentioned in section 2.4. We can overcome this problem with the design shown in Figure 3.4(d). The arms with oppositely directed (perpendicular to z-axis) have been brought closer so that the fields produced by these arms cancel in the far-field. This arrangement also minimizes the length of the arms that are parallel but distant from z-axis.

This design has been simulated in Agilent ADS and results show that traveling waves are indeed being setup in the structure. Figure 3.5 shows that current density reduces as the distance from the feed point increase. This design has been fabricated on a substrate with relative dielectric permittivity of 2.6 (see Figure 3.6). Three such antennas have been used in a setup as shown in Figure 3.7 to form a tri-polarized traveling wave antenna. The return loss and coupling between two meanderline traveling wave antenna elements in this setup is shown in Figure 3.8. The return loss is below -10 dB and the coupling is below -15 dB in the frequency range $f_1 = 7.3$ GHz to $f_2 = 8.5$ GHz and hence satisfactory for our purpose.

3.4 Channel Measurements

The channel measurement system comprises of N antenna elements at the transmitter, M antenna elements at the receiver and Q scatterers. The direct path between the transmitter and the receiver is blocked to simulate a non-line of sight (NLOS) channel. The scatterers are placed in the azimuthal plane at randomly generated angles, (ϕ), with uniform probability density function. This is a popular model for azimuthal distribution of scatterers [13]. The number of scatterers ($Q = 16$) was chosen based on the average number of paths between the transmitter and receiver as reported in [14]. The aim of channel measurements is to determine the channel matrix for this $M \times N$ MIMO system.

The schematic for the measurement test-bed is shown in Figure 3.9. Consider the i-th receiver at port 2 and the j-th transmitter at port 1. Let V_1 and V_2 represent the total voltages at ports 1 and 2, respectively. By definition

$$h_{ij} = \frac{V_2}{V_1} = \frac{V_2^+ + V_2^-}{V_1^+ + V_1^-} \tag{3.1}$$

where the "+" and "-" superscripts indicate incident and reflected voltages, respectively. Let

$$a_1 = \frac{V_1^+}{\sqrt{Z_{01}}}, a_2 = \frac{V_2^+}{\sqrt{Z_{02}}}, b_1 = \frac{V_1^-}{\sqrt{Z_{01}}}, b_2 = \frac{V_2^-}{\sqrt{Z_{02}}} \tag{3.2}$$

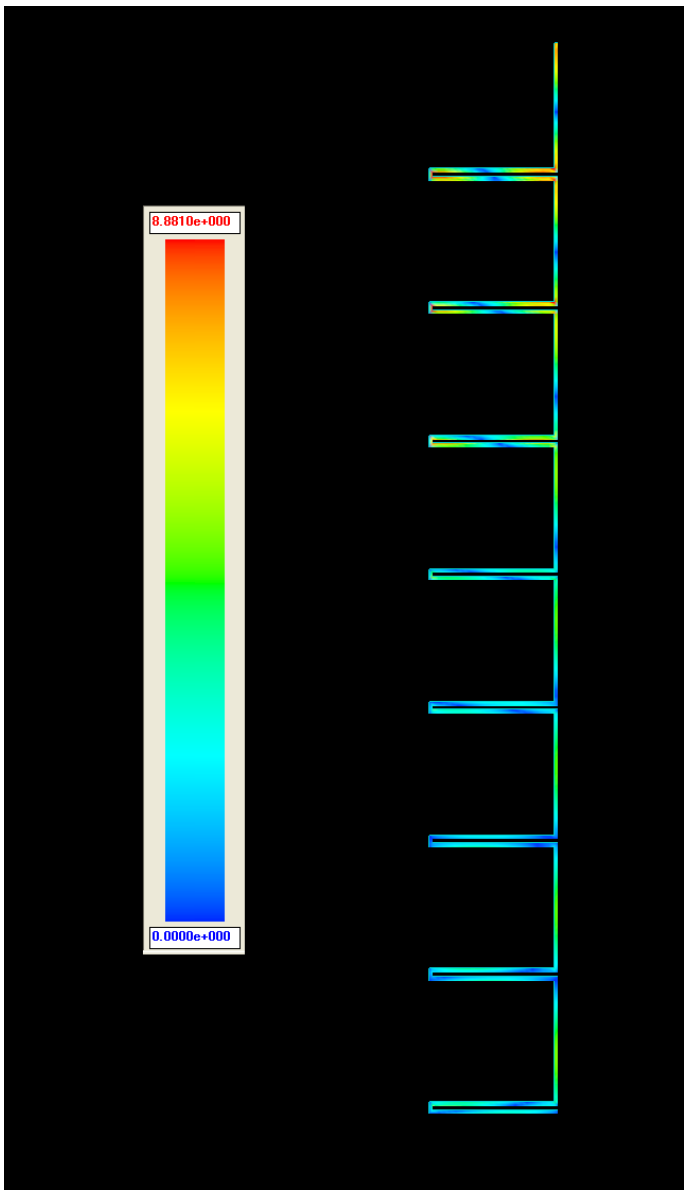

Figure 3.5: Current density on Meanderline traveling wave antenna

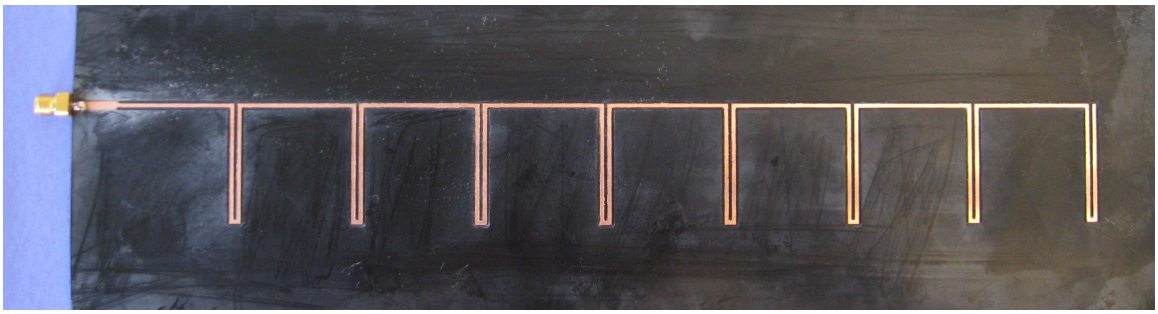

Figure 3.6: Fabricated prototype of meanderline traveling wave antenna

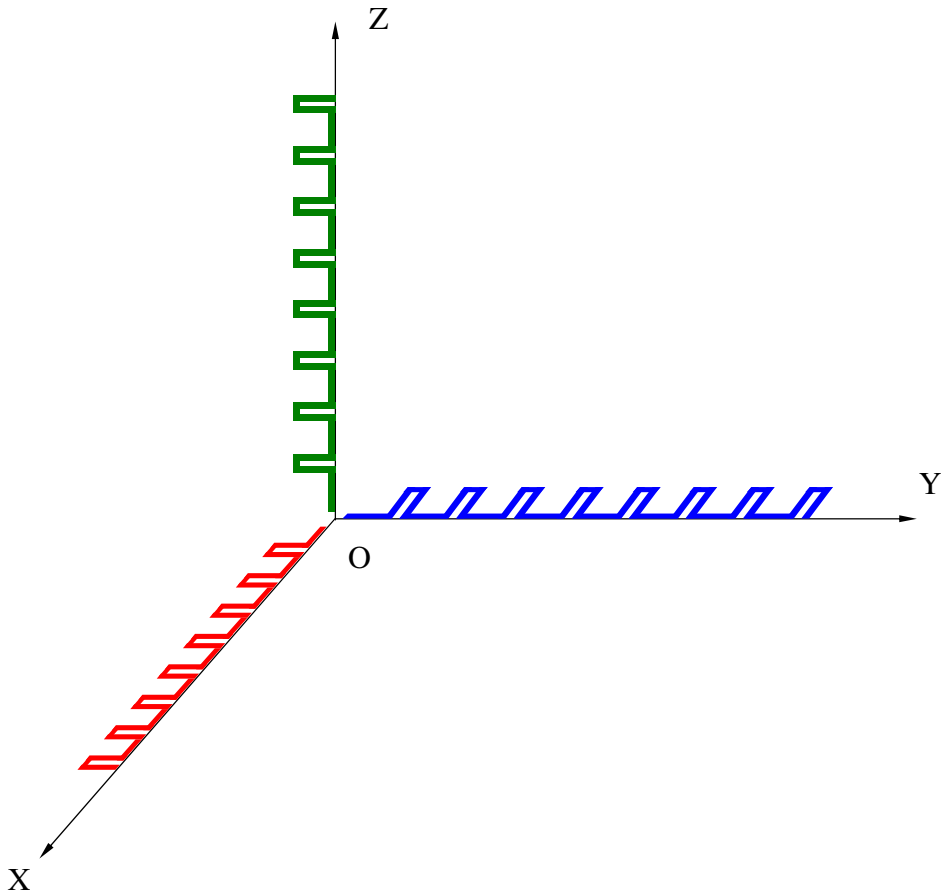

Figure 3.7: Arrangement of dipoles to form a tri-polarized traveling wave antenna

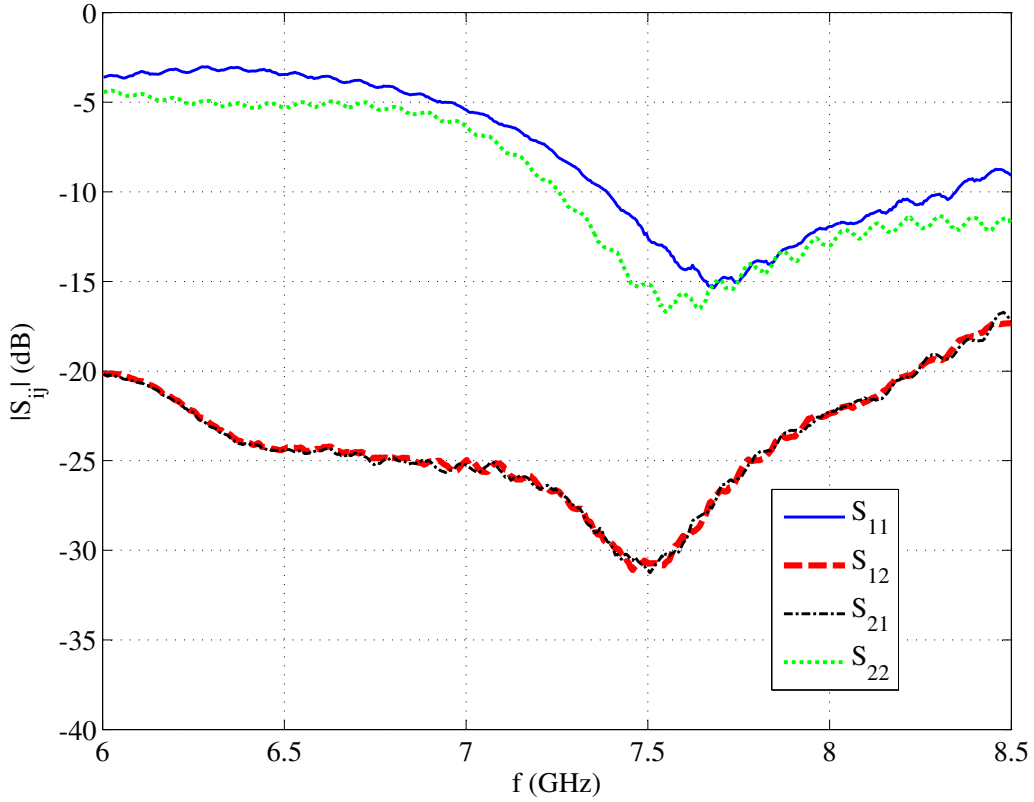

Figure 3.8: Return loss and coupling between elements of tri-polarized traveling wave antenna

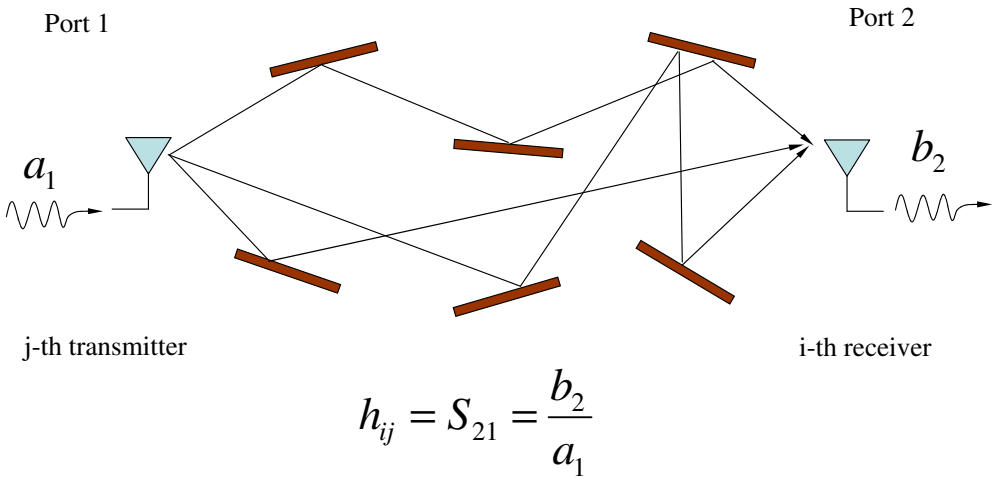

Figure 3.9: Schematic representation of experimental setup

where Z_{01} and Z_{02} are the characteristic impedances of ports 1 and 2, respectively. Substituting, (3.2) in (3.1), we get

$$h_{ij} = \frac{(a_2 + b_2)\sqrt{Z_{01}}}{(a_1 + b_1)\sqrt{Z_{01}}}. \tag{3.3}$$

Since the antennas are matched to $Z_{01} = Z_{01} = 50\Omega$ we can consider the traveling voltage waves to be essentially the total voltages at the respective ports, i.e., $a_2 = b_1 = 0$. Therefore, we have

$$h_{ij} = \frac{b_2}{a_1} = S_{21}. \tag{3.4}$$

According to the above equation, the i,j-th entry of the channel transfer matrix **H** can be found by measuring transfer S-parameter, S_{21}, while the other antennas are terminated in 50Ω loads.

The S-parameter measurement has been facilitated by the use of Agilent 87130A-K01 Switching Interface that can be controlled by Agilent E5071B ENA Series Network Analyzer using the VISA library functions through the Agilent 82357A USB/GPIB Interface. The Switching Interface can extend the capability of Network Analyzer to handle a maximum of 6 antennas at both its ports. This means that upto 6×6 MIMO systems can be emulated. At any given time only one pair of transceiver ports in the Switching Interface is active while the rest are terminated in 50Ω loads. A Visual Basic program has been

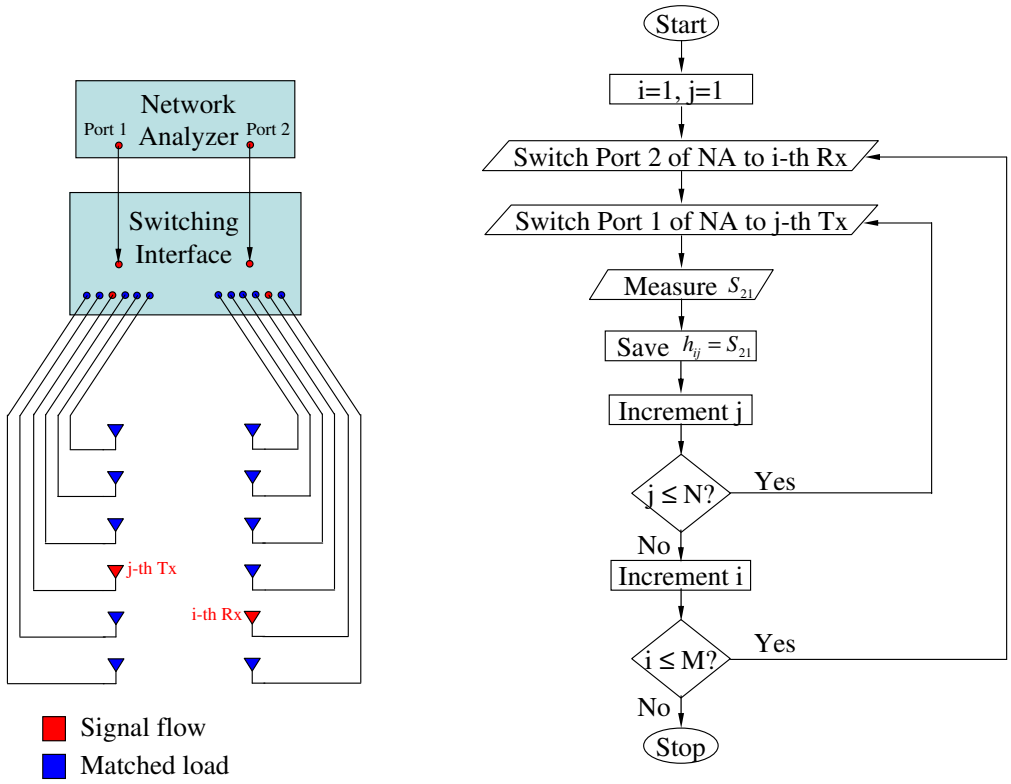

Figure 3.10: Algorithm for measurement of channel matrix **H**

written that automatically cycles between all possible pairs of transceiver ports, makes the measurement and saves the S-parameter data in appropriate directories for post-processing. The algorithm used in the program for an $M \times N$ system is depicted in the flowchart shown in Figure 3.10. The ports and the antennas shown in red color have signal flowing through them while those in blue have been terminated in 50Ω loads.

Chapter 4

Capacity Calculations from Simulation and Measurement

4.1 Introduction

In this chapter, we study the benefits of polarization from the channel capacity point of view. Channel capacity is a very significant parameter for MIMO channels as it is the upper bound on the amount of information that can be reliably transmitted over the channel. Krishnamurthy et al [24, 25] used fabricated prototypes of vector antennas and then compared their capacity to that of spatial array antennas. We do a similar capacity calculation of the tri-polarized antennas described in chapter 3. We evaluate the capacity offered by tri-polarized antennas in linear array configuration and compare that to their uni-polarized counterparts. For comparison purposes, we also present the channel capacity gains from simulation for the case of ideal infinitesimally small antennas.

4.2 Channel Model

In this section, we describe how to calculate the channel state information for the case of infinitesimally small antennas. For this we require a channel model to evaluate the channel matrix. An exhaustive survey of channel models is available in [26, 27]. However, for the purpose of this study, we found the model proposed by Zwick et al [14, 15] most appropriate because it explicitly models the directional location of scatterers and can be

easily combined with the radiation pattern of antennas to generate the channel matrices

$$\begin{aligned}\mathbf{\Phi}(t,\tau,\Omega_T,\Omega_R) = \sum_{i=1}^{Q(t)} \mathbf{\Gamma}_i(t) u(\tau-\tau_i(t))\times \\ \delta(\Omega_T-\Omega_{T,i}(t))\delta(\Omega_R-\Omega_{R,i}(t))\end{aligned} \tag{4.1}$$

which describes the cumulative effect of Q multi-path components where the i-th path originates towards the direction $\Omega_{T,i}$ from the transmitter, the θ and ϕ components of the field get transformed by a scatterer through the transfer matrix $\mathbf{\Gamma}_i$ and reaches the receiver from the direction $\Omega_{R,i}$. The dispersion encountered in the path is described by the function $u(\cdot)$ and delay is τ_i. All these parameters are functions of time t.

The MIMO channel response then becomes $\mathbf{H} = (h_{ij})$ where

$$h_{ij}(t,\tau) = \int\int \mathbf{C}_{R,i}^T(t,\Omega_R)\mathbf{\Phi}(t,\tau,\Omega_T,\Omega_R)\mathbf{C}_{T,j}(t,\Omega_T)d\Omega_T\Omega_R \tag{4.2}$$

where $\mathbf{C}_{T,j}$ and $\mathbf{C}_{R,i}$ are the radiation patterns of the j^{th} transmit and i^{th} receive antennas respectively.

The above model is very detailed; therefore, we make some simplifying assumptions to retain only its salient features. We assume that the number of paths $Q(t)$ does not vary over time and the channel is not frequency selective (i.e. $u(\tau) = \delta(\tau)$). We considered 'Non Line Of Sight' (NLOS) scenarios, which is typical of indoor channel environments, and a maximum delay relative to mean path delay $\tau'_{max} < 300\ ns$ at 2.5 GHz [15]. Therefore we assume that the multi-path components arrive at the receiver at the same time. The elements of $\mathbf{\Gamma}_i(t)$ were generated using zero mean complex normal random variables, with co- and cross- polarization weights given by $X_{\theta\theta} = 1, X_{\theta\phi} = 0.1, X_{\phi\theta} = 0.1, X_{\phi\phi} = 1$. The following probability density functions were used for the directions Ω_T and Ω_R

$$p(\theta) = \begin{cases} \frac{\sin(\theta)}{2} & \theta \in [0,\pi) \\ 0 & \text{otherwise} \end{cases} \tag{4.3}$$

$$p(\phi) = \begin{cases} \frac{1}{2} & \phi \in [0,2\pi) \\ 0 & \text{otherwise} \end{cases} \tag{4.4}$$

This formulation of the channel model can be used for the calculation of the theoretical capacity of a system employing uniformly spaced tri-polarized antennas, performed in Section 4.3.

4.3 Capacity Calculations

We consider the following model for the received signal

$$\mathbf{r} = \sqrt{\frac{\rho}{l}}\mathbf{H}\mathbf{x} + \mathbf{n} \tag{4.5}$$

where $\mathbf{H}$ represents the channel matrix, $\mathbf{x}$ is the transmitted signal and the components of the noise vector, $\mathbf{n}$ are independent and identically distributed $\sim CN(0,1)$. We consider the case where perfect channel state information (CSI) is available at the receiver but not at the transmitter. The ergodic channel capacity for an $l \times l$ MIMO system under the constraint of equal power distribution across all transmitting antennas, at SNR per receive antenna, ρ is given by [3]

$$C = \log_2 \left| I + \frac{\rho}{l}\hat{\mathbf{H}}\hat{\mathbf{H}}^{\dagger} \right| \tag{4.6}$$

where $|\cdot|$ denotes the determinant of a matrix and $[\cdot]^{\dagger}$ the conjugate transpose operation. The CSI matrix, H, is a function of frequency, f, for broadband MIMO systems. Therefore, the capacity of these systems is found by integrating 4.6 over the frequency range of interest

$$C = \frac{1}{f_H - f_L} \int_{W_L}^{W_H} \log_2 \left| I + \frac{\rho}{l}\hat{\mathbf{H}}(f)\hat{\mathbf{H}}^{\dagger}(f) \right| df \tag{4.7}$$

where f_L and f_H denote the lower and higher ends of the frequency range of interest. The CSI measured by the network analyzer is available only at discrete points in the frequency domain $f_n, n = 1, 2, \ldots, N$. In this case, the capacity can be approximated by [28], [29]

$$C \approx \frac{1}{N} \sum_{n=1}^{N} \log_2 \left| \mathbf{I} + \frac{\rho}{l}\hat{\mathbf{H}}(f_n)\hat{\mathbf{H}}(f_n)^{\dagger} \right| \quad \text{bits/s/Hz} \tag{4.8}$$

Note that the channel matrices in the above capacity calculation have been normalized according to

$$\hat{\mathbf{H}}(f_n) = \mathbf{H}(f_n)/\alpha \tag{4.9}$$

where α is the root-mean-squared value of the fading path gains that can be calculated from the tri-polarized CSI, $\mathbf{H}^{tri}(f_n)$ by the following formula

$$\alpha = \sqrt{\frac{\sum_{i=1}^{l}\sum_{j=1}^{l}\sum_{n=1}^{N} |H_{ij}^{tri}(f_n)|^2}{l^2 N}} \tag{4.10}$$

to remove the effect of pathloss.

A measure of performance gain by using polarized antennas is the ratio of capacity using tri-polarized antennas to the capacity using just uni-polarized antennas. As there could be three possible directions for uni-polarized antennas we take the average of capacity for each polarization. Therefore, the gain is given by

$$G = \frac{E(C_t)}{\frac{1}{3}\sum_{i=x,y,z} E(C_i)} \tag{4.11}$$

where $E(\cdot)$ denotes the expectation operation and $i = t, x, y, z$ for the tri-polarized, x, y, z-polarized cases respectively.

4.3.1 Narrowband Antennas

In this section, we describe the capacity gain results for narrowband tri-polarized antenna systems with dipole elements. The transmitter consists of two tripoles separated by a distance of 24 cm which results in $kL \approx 31$. The receiver is similar to the transmitter and is placed in the far field of the transmitter. Figure 4.1 shows the measured capacity gain using the setup described in section 3.4. It also shows the gain in capacity v/s SNR for a uniform linear array of the same length with different number of infinitesimally small antennas using the channel model described in (4.1). It can be seen that there is approximately three fold increase in capacity for different number of antennas for a range of SNRs. For example, the gain for the system simulated using 2 tripoles each at the transmitter and the receiver varies from 2.7 to 2.95 for SNR from 0 to 100 dB respectively when the number of paths, $Q = 16$. At 25 dB SNR, $E(C_t)/\max E(C_i) = 2.88$ where as $G = 2.93$, therefore $E(C_x), E(C_y)$ and $E(C_z)$ are contributing equally to the gain G in (4.11). Figure 4.2 compares the ergodic capacity of the 6×6 channel for a spatial array to a vector array of two tripoles. The noise level is less than -80 dB whereas the measurements show that the most of the channel measurements readings above -60 dB. Moreover, to verify that this noise was not adversely affecting the measurements, channel measurements were done for the same scattering environment. Figure 4.3 shows the capacity plots for 20 such measurements. The mean capacity at 10 dB SNR is 15.3 bps/Hz and the variance is 0.058 bps/Hz.

4.3.2 Broadband Antennas

In this section, we describe the capacity gain results for two types of broadband antenna systems, namely the ultrawideband antenna system designed by Rajagopalan [12]

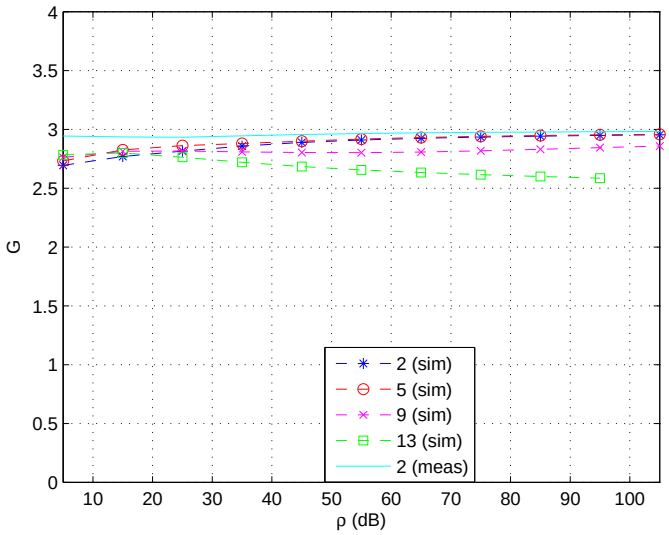

(a) $Q = 16$

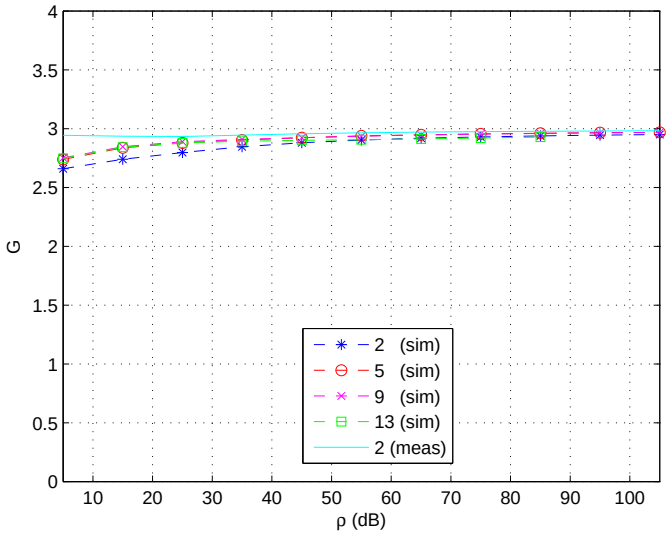

(b) $Q = 35$

Figure 4.1: Average capacity gain v/s SNR for a uniform linear array of 2,5,9 and 13 tri-polarized antennas

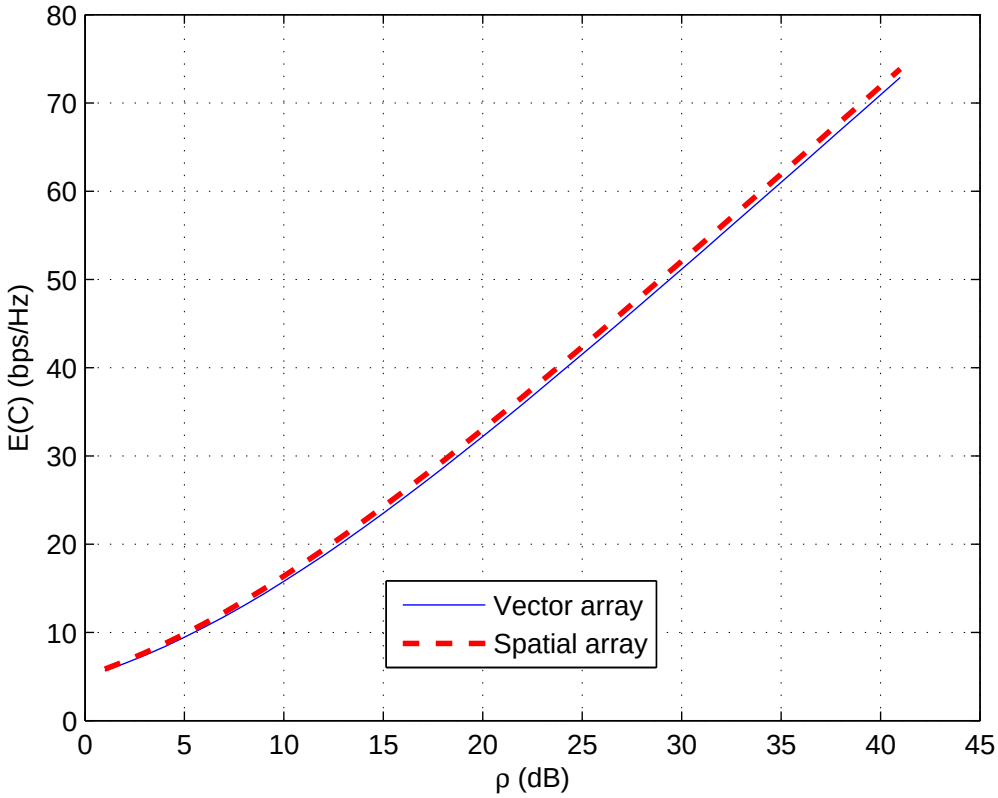

Figure 4.2: Capacity of a 6×6 system v/s SNR for (a) vector array of two tripoles and (b) spatial array of 6 elements

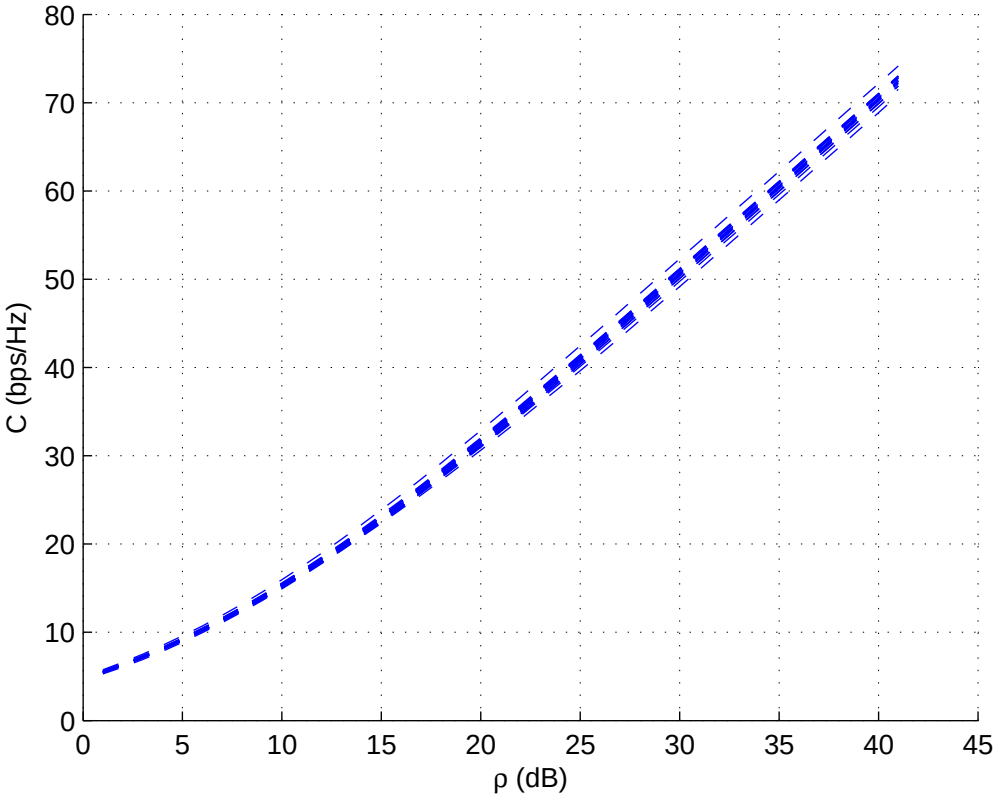

Figure 4.3: Capacity of a 6×6 system for 20 successive measurements with same scattering environment and transmitter and receiver being arrays of two tripoles

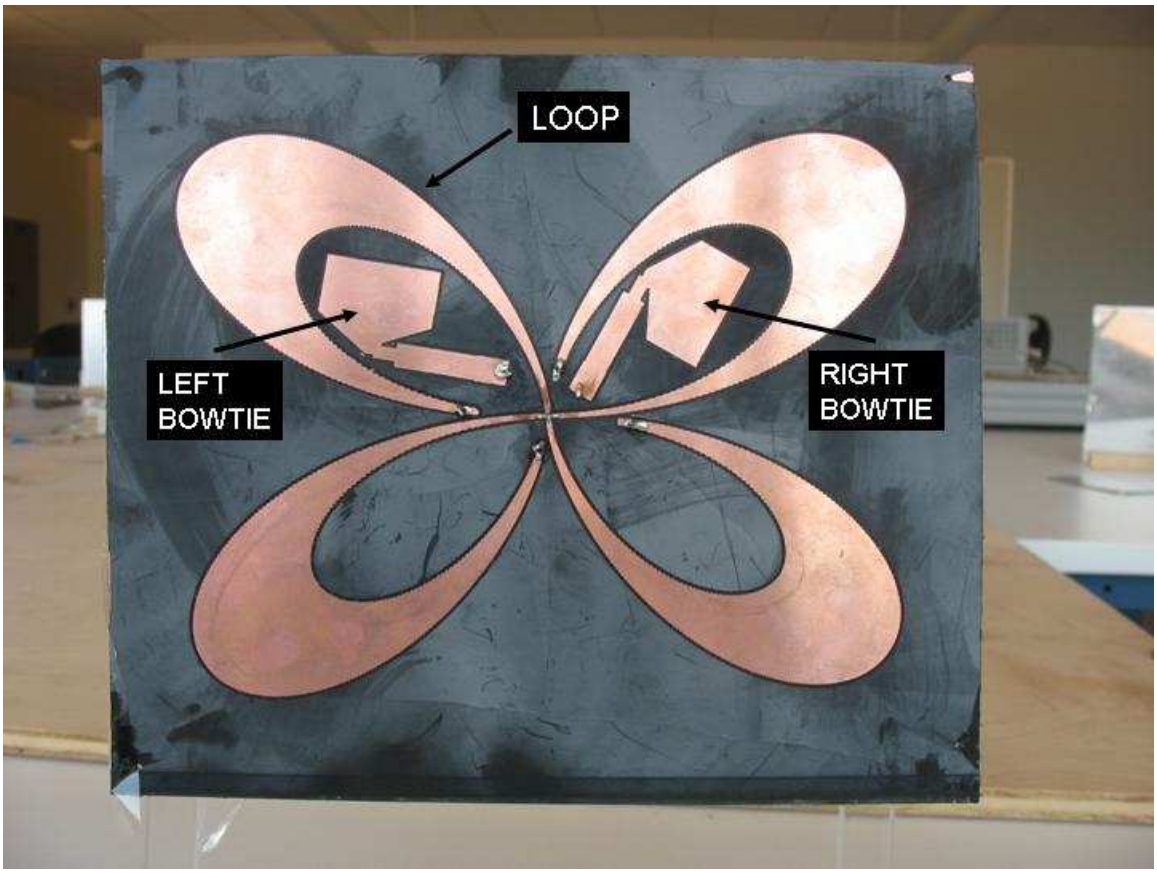

Figure 4.4: Three-element Ultrawideband vector antenna

and the meanderline antenna system described in section 3.3. Ultrawideband is a radio technology used for short-range high-bandwidth communications. The Federal Communications Commission classifies a transmission system as ultrawideband if its signal bandwidth exceeds 500 MHz or 20% of the center frequency. Figure 4.4 shows the three-element ultrawideband vector antenna used in this study. The bowtie is the broadband equivalent of electrical dipole and the loop is the broadband equivalent of magnetic dipole. The antenna operates in the frequency range $f_1 = 3.6$ GHz to $f_2 = 8.5$ GHz. In this range, the return loss of loop is below -8 dB and that of both the bowties is below -10 dB. Mutual coupling between any pair of elements is below -15 dB.

Figure 4.5 shows the gain in capacity v/s SNR for the 3×3 UWB tri-polarized antenna systems. It also show the gain for 6×6 traveling wave antenna system (linear array of two tri-polarized meanderline antennas at the transmitter as well as the receiver). As in

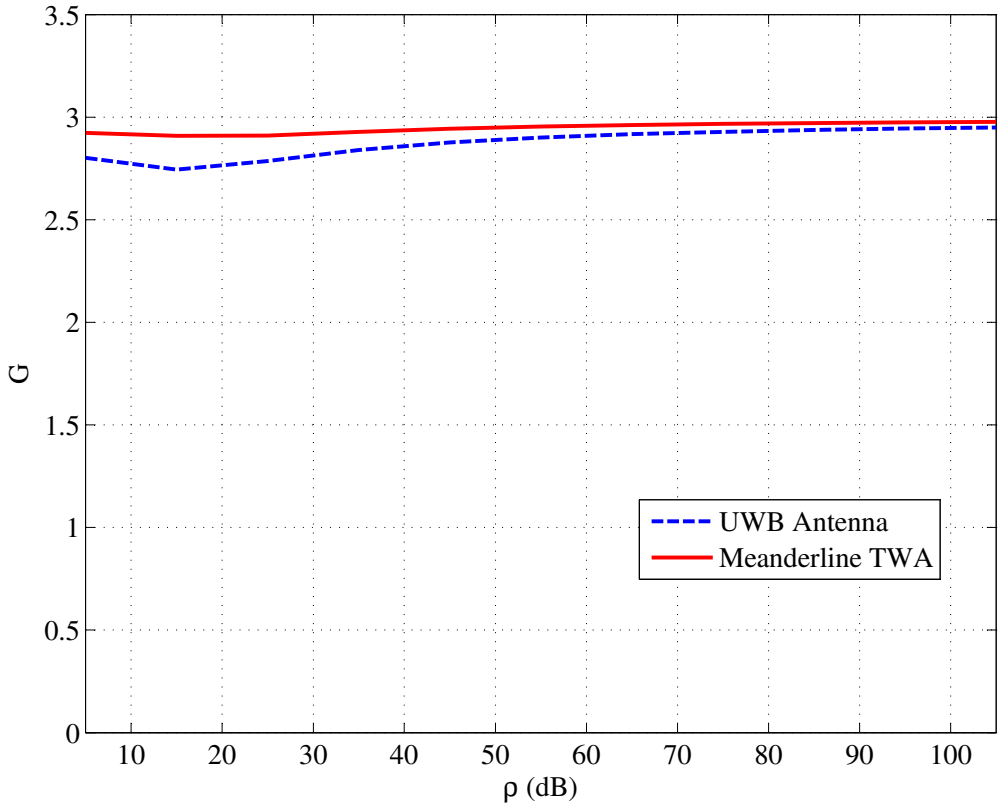

Figure 4.5: Average capacity gain v/s SNR for UWB and Meanderline traveling wave antenna elements

the case of narrowband dipole antennas, the gain is approximately three-fold for a range of SNRs. The gain varies from 2.74 to 2.95 for UWB antenna and 2.9 to 2.97 for meanderline antenna.

Chapter 5

Frequency Selective Surfaces

5.1 Introduction

Frequency Selective Surfaces (FSSs) are periodic arrays (usually two dimensional) often in the form of printed structures on substrate or apertures in a conducting plane. These surfaces behave as filters for incident electromagnetic waves based on frequency and polarization of incident field [5]. The resonant frequency as well as bandwidth of the FSS depends on the unit antenna element used in the array.

In this study we consider FSSs that are embedded on a fabric. The aim is to recognize the presence of the fabric from a remote location by illuminating it with microwave radiation. The (passive) antennas on the fabric are designed so the reflected signal from the fabric contains some distinct signature that helps in recognizing the fabric. In particular, we study the benefits that the use of vector antennas can provide when embedded on fabrics. Vector antennas offer polarization and pattern diversity which has been used in communication systems to provide higher capacity and improved source localization [1, 30].

5.2 Formulation of the problem

A monostatic antenna is used for transmitting as well as receiving signals. This transceiver antenna is connected to the network analyzer. A fabric embedded with passive antennas is placed at a distance r in the far-field of the monostatic antenna. Two sets of measurements were done to calculate the signature bearing signal, $x(f)$. Let S_{11}^{free} and S_{11}^{fab} denote the return loss measurements in the absence and presence of the fabric respectively.

Table 5.1: MSE for FSS of open and shorted dipoles placed orthogonally with dipole transceiver

Transceiver aligned to	r	MSE $\bar{X}$	MSE (dB) $10\log_{10}(\bar{X})$
Shorted dipole	30 cm	0.0017	-27.69
Shorted dipole	80 cm	1.09×10^{-4}	-39.59
Open dipole	30 cm	3.2137×10^{-5}	-44.92

A metric that carries the signature due to fabric is given by

$$x(f) = |S_{11}^{fab}(f)|^2 - |S_{11}^{free}(f)|^2 \tag{5.1}$$

To quantify the benefits of using these signatures we consider the mean signal energy (MSE), $\bar{X}_i$ over the bandwidth of interest

$$\bar{X}_i = \frac{\int_{f_1}^{f_2} |x_i(f)| df}{f_2 - f_1} \tag{5.2}$$

5.3 Measured Results

5.3.1 Single Transceiver

We use a single dipole as a transceiver. The vector antenna consists of an open and a shorted dipole placed orthogonally to each other. The dimensions of the unit element and the fabricated protoype are shown in Figure 5.1. The shorted dipole is supposed to reflect while the open dipole is supposed to transmit most of the incident energy. The measured signature signals for r=30 and 80 cm are shown in Figure 5.2 when the transceiver is aligned along open and short dipoles. Table 5.1 summarizes the MSE for these cases. It can be observed that at 30 cm the MSE is 17.23 dB higher when the transceiver is aligned with the shorted dipole as compared to the open dipole as expected. In case the alignment of the antennas on the fabric is not know a priori, we can use a circularly polarized antenna as transceiver. In this case, MSE will be high only when the circularly polarized wave aligns with the shorted dipole. This high change in MSE will occur twice in every cycle of the polarized wave and can be used to ascertain the presence of the FSS.

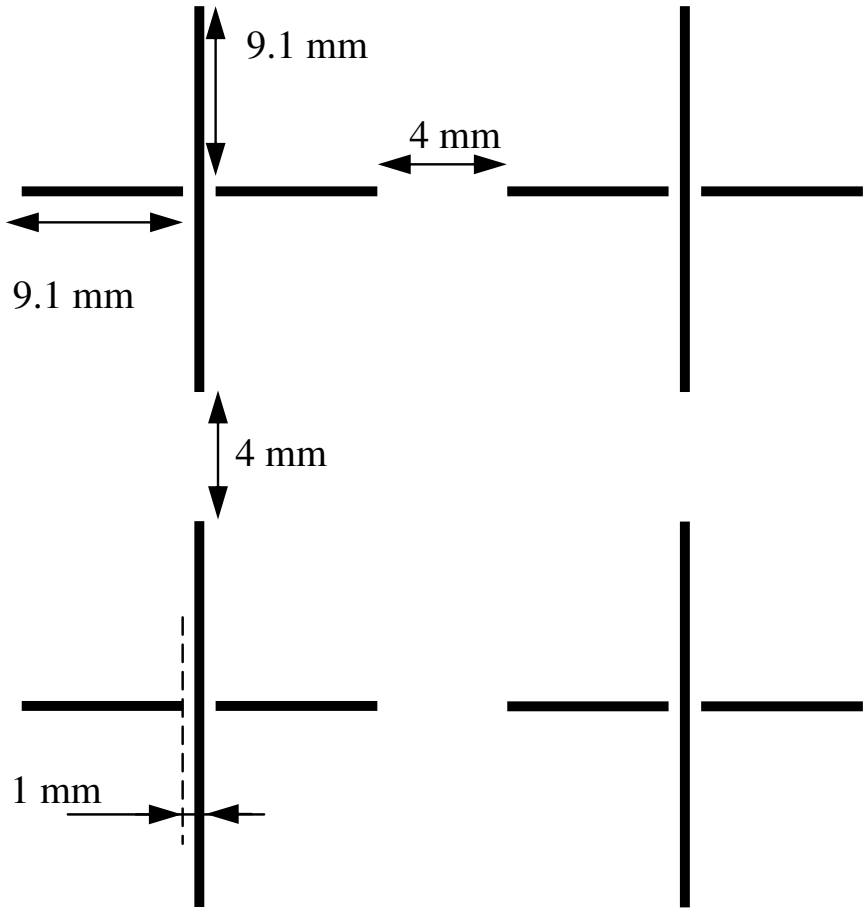

Figure 5.1: Vector antenna array embedded in fabric

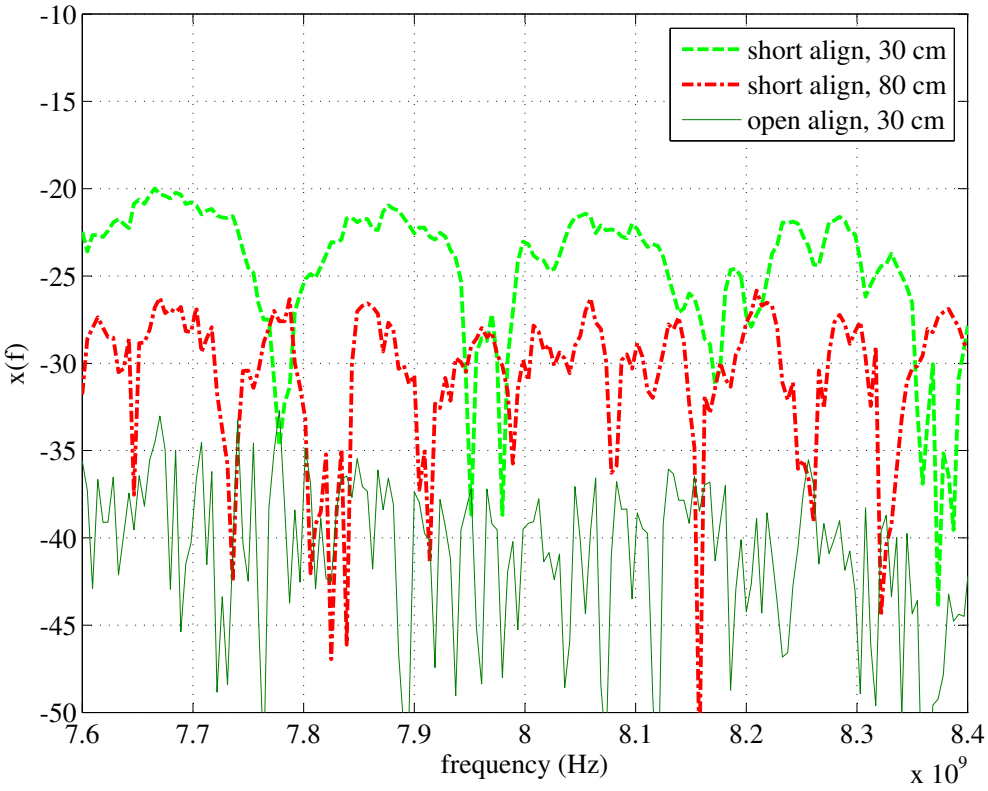

Figure 5.2: Signature signal from vector antenna array for different alignments

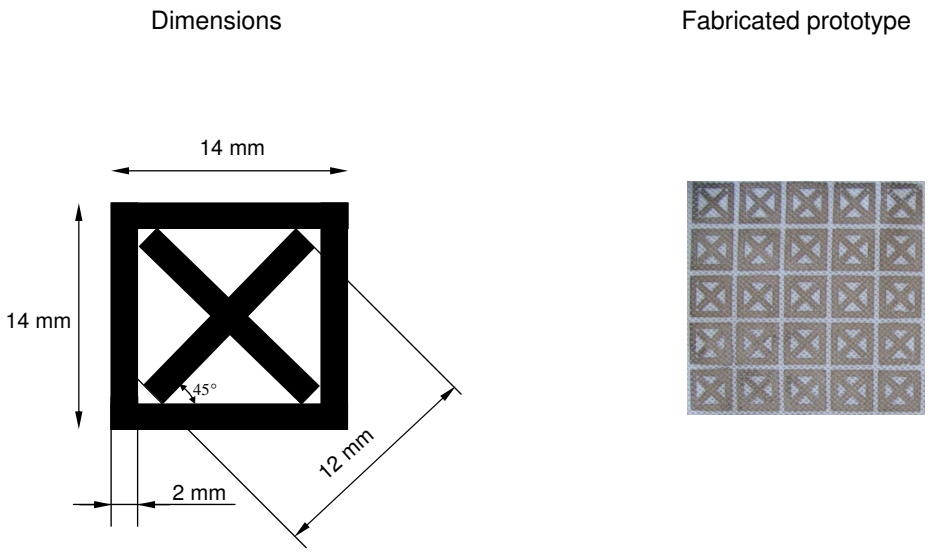

Figure 5.3: Vector antenna array embedded in fabric

5.3.2 Multiple Transceivers

If vector antennas are used in the monostatic transceiver as well as the fabric we will receive multiple signals with signatures, $x_i(f)$ corresponding to each antenna element of the vector antenna system.

The vector antenna used in this study consists of a square loop and two orthogonal dipoles shorted at the center. The vector antenna was designed on the fabric using screen printing process with silver ink. The inter-element spacing in the two dimensional array is half-wavelength at the center frequency of 8 GHz. The geometry, dimensions and fabricated prototype are shown in Figure 5.3. Two types of transceivers were used - (1) a square loop and (2) a half-wavelength dipole. For comparison we use a uni-polarized system as reference. This system uses 2-dimensional array of dipoles (see Figure 5.4) on a fabric and a dipole as transceiver.

All the antennas were first simulated in Agilent ADS software and then fabricated on a substrate with $\epsilon_r = 2.6$. Figure 5.5 shows the free space return loss of the dipole and the loop used in the transceiver. The return loss for the loop and the dipole are below -8 dB and -10 dB, respectively, in the frequency range $f_1 = 7.8$ GHz to $f_2 = 8.2$ GHz.

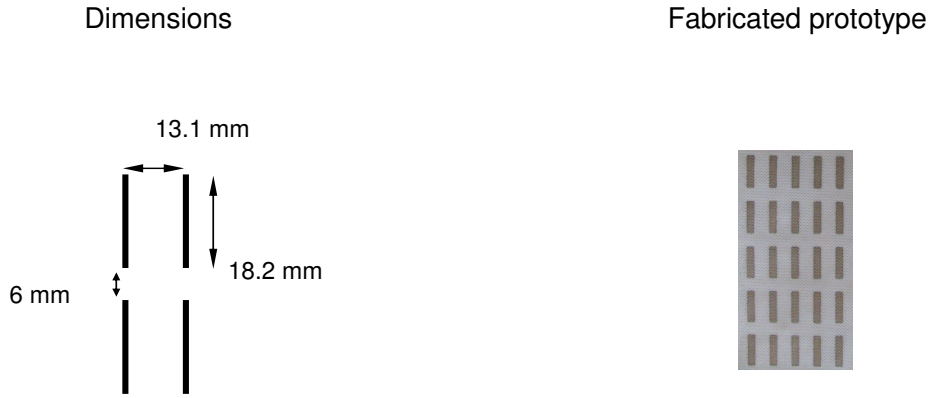

Figure 5.4: Dipole array embedded in fabric

Table 5.2: MSE for FSS of loop and orthogonal shorted dipole antennas with perfectly aligned loop and dipole transceivers

Array element	Transceiver	MSE $\bar{X}$	MSE (dB) $10\log_{10}(\bar{X})$
Vector antenna	Dipole	0.0023	-26.38
Vector antenna	Loop	0.0034	-24.68
Dipole	Dipole	0.0019	-27.21

The measured signatures obtained for vector antenna and dipole FSS when the distance between the fabric and transceiver is 30 cm are shown in Figure 5.6. Table 5.2 summarizes the MSE for different combinations of fabric antennas and transceivers. It can be observed that vector antenna fabric with dipole and loop as transceiver provides 1 dB and 2.5 dB gain respectively with respect to the conventional dipole array. These individual gains can be further improved if additional signal processing is used to combine the signature received by dipole and loop antennas. The simplest processing that can be used on signatures is to combine the two signals

$$y(f) = x_1(f) + x_2(f) \tag{5.3}$$

By combining the signal signatures from dipole and loop antennas, the MSE is raised to $\bar{Y} = -23.1$ dB which is a gain of almost 4 dB with respect to using the conventional dipole

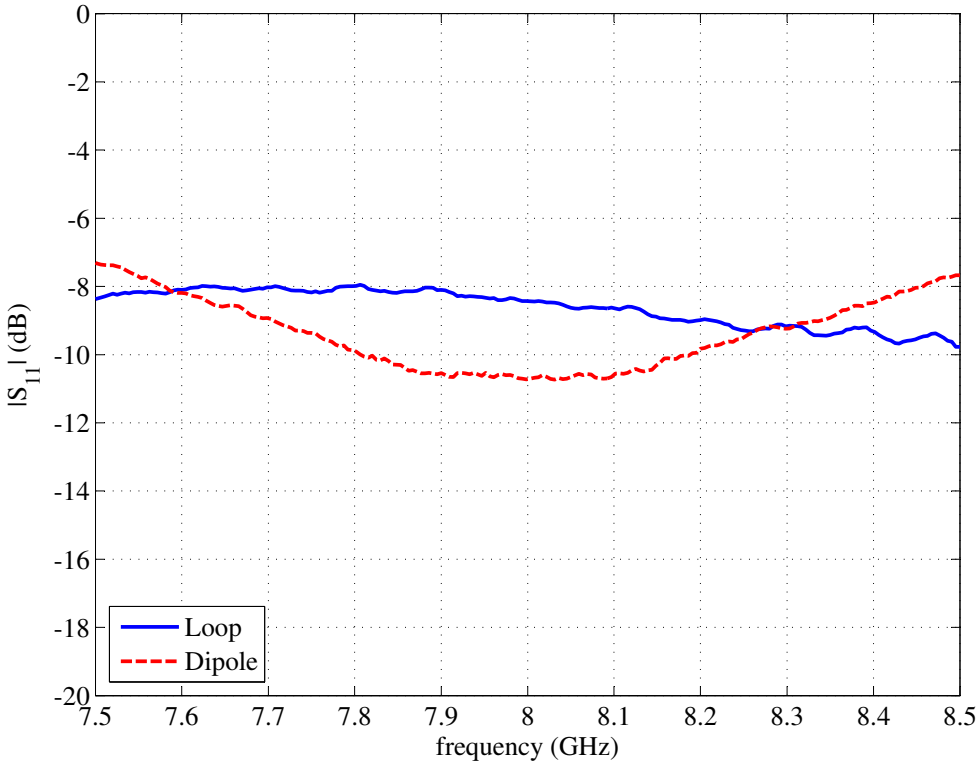

Figure 5.5: Return loss of the loop and dipole transceivers

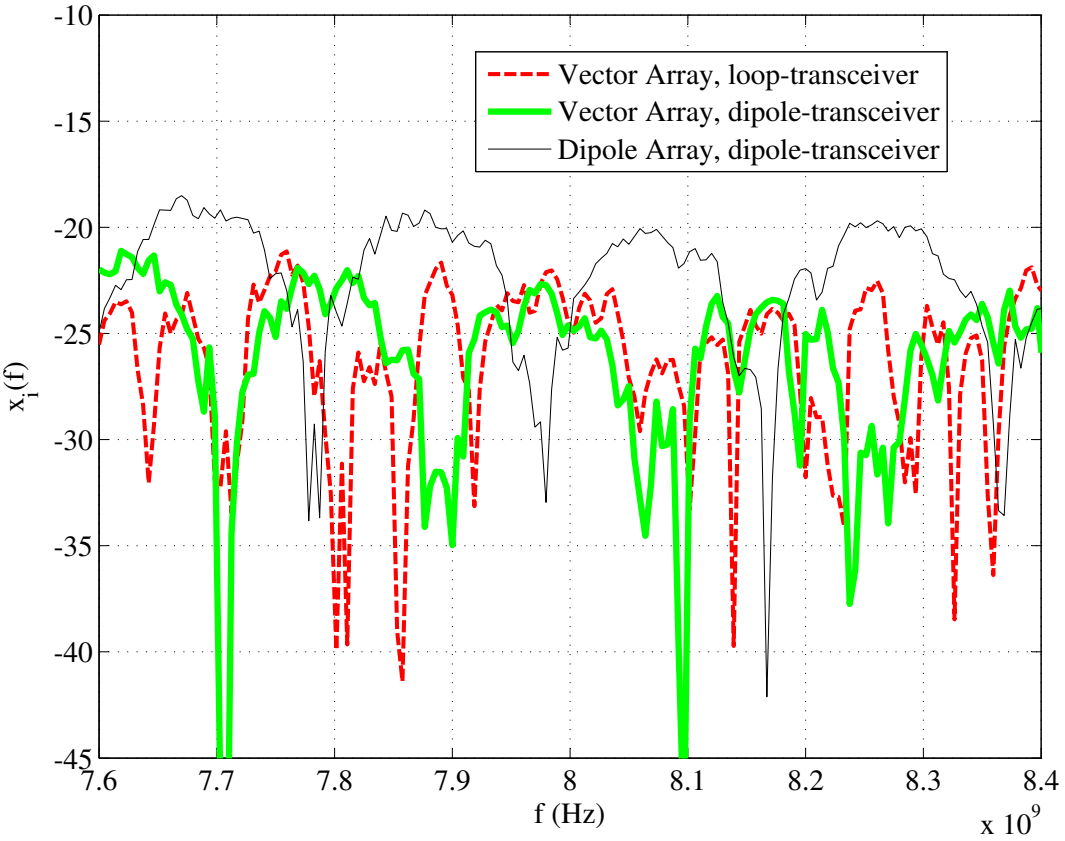

Figure 5.6: Measured signatures for vector antenna and dipole FSS

Table 5.3: MSE for FSS of loop and orthogonal shorted dipole antennas with maximally misaligned loop and dipole transceivers

Array element	Transceiver	Misalignment	MSE $\bar{X}$	MSE (dB) $10\log_{10}(\bar{X})$
Vector antenna	Dipole	45°	0.0013	-28.86
Vector antenna	Loop	45°	0.0034	-24.68
Dipole	Dipole	90°	4×10^{-6}	-53.92

array.

The above results are valid only when there is exact alignment between the vector antennas on fabric and the transceiver. The orientation of the fabric is unknown at the transceiver which can cause misalignment between them. To study the impact of misalignment on the performance of vector antennas we consider the worst case scenario, that is maximum misalignment. Due the symmetry of the vector antenna design the maximum misalignment with the transceiver can be 45° only while for the conventional dipole array it can be 90°. Table 5.3 summarizes the MSE for different cases. It can be observed that when the vector antenna is illuminated by loop and dipole the loss in MSE is 0 dB and 2.5 dB respectively with respect to perfectly aligned case. This loss is quite small as compared to the 26.7 dB loss for the conventional dipole array illuminated by dipole antenna. It is also interesting to note that even in the case of misalignment the MSE does not change when the square loop is used as a transceiver. This is due to the fact that even tough the shape of the loop is square it is actually behaving like a circular loop.

5.4 Conclusion

In this chapter, we proposed two types of vector antenna systems to be used a unit elements of FSS. The two element vector antenna (orthogonal open and shorted dipoles) is used with a dipole transceiver. As confirmed by measured results at 8 GHz, the fabricated prototype is capable of providing an alignment dependent signature signal. The three element vector antenna (two orthogonal dipoles and a square loop) has been used with two transceivers (dipole and loop). A prototype design fabricated to work at 8 GHz was tested. Measurement results show that vector antennas provide a higher MSE as compared to conventional dipole antennas. The multiple signatures can be obtained by using loop and

dipole antennas at the transceiver. These multiple signatures can be combined to provide even higher MSE (≈ 4 dB) as compared to the system with two dimensional dipole array and dipole transceiver. The vector antenna system is also much more resistant to misalignment with the transceiver.

Chapter 6

Conclusion and Future Work

In this work, we have studied vector antennas and their applications. In particular, the performance of tri-polarized vector antennas has been evaluated through three different approaches - theoretical analysis, computer simulation and experimental measurements. All the three approaches lead to a consistent result that vector antennas can provide a three-fold increase in channel capacity.

Linear arrays of tri-polarized antenna elements provide a three-fold increase in the degrees of freedom as compared to analogous arrays of uni-polarized antennas. Three different types of antenna elements have been investigated in this analysis, namely, infinitesimally small antennas, finite length dipole and long wire traveling wave antenna. For experimental investigation, two types of tri-polarized antenna systems have been designed. The narrowband system consists of CPS-fed co-located dipole elements and the broadband system consists of meanderline traveling wave antenna elements. These antennas have been used in linear array MIMO configuration. From experimental channel measurements we found that they indeed provide three-fold increase in capacity as compared to analogous arrays of uni-polarized antennas. Therefore, these vector antennas are compact alternatives for use in MIMO systems as compared to spatially separated linear arrays.

We also found vector antennas to be very useful for Frequency Selective Surfaces. These antennas, when embedded on fabrics as unit elements, act like FSS and provide certain signatures that can help in identifying its presence. We found that vector antenna FSS provide higher reflected energy and are much more resistant to misalignment compared to uni-polarized antenna FSS.

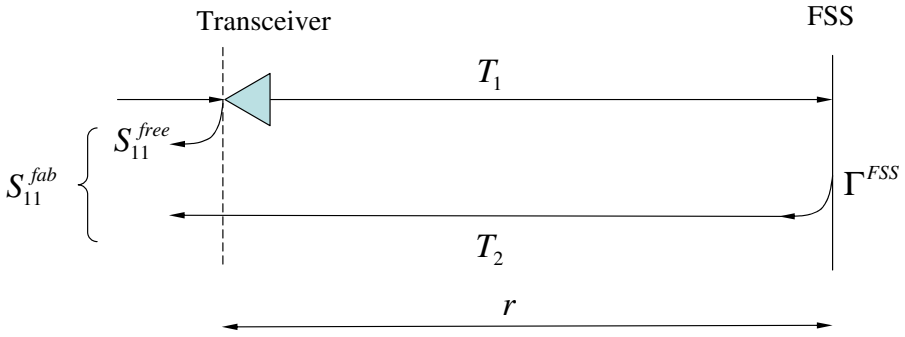

Figure 6.1: Estimation of reflection from FSS

6.1 Future Work

6.1.1 Degrees of Freedom

As a part of this study, we analyzed the degrees of freedom of only linear arrays of vector antennas. It is of interest to extend this analysis for other types of array geometries like circular and spherical arrays. For these geometries the analysis presented in this work becomes cumbersome and mathematically intractable. A degrees of freedom analysis for uni-polarized arrays with these geometries appears in [8] but the tri-polarized case has been analyzed only heuristically.

6.1.2 Frequency Selective Surfaces

The present work on integrating vector antennas on fabrics to form Frequency Selective Surfaces raises some important fundamental questions. It is of interest to develop a model based on electromagnetic theory that correctly estimates the reflected signal from the FSS. In this section, we describe the current setup that may serve as guideline for future investigation. Figure 6.1 shows the experimental setup. As mentioned in chapter 5, we can measure the reflection coefficient of the transceiver in free space (S_{11}^{free}) and in the presence of the fabric (S_{11}^{fab}). We also know from Friis transmission equation that

$$T_1 = T_2 = \sqrt{\frac{G_{ant} G_{FSS} \lambda^2}{(4\pi r)^2}} e^{ikr} \tag{6.1}$$

where r is the distance between the transceiver and the FSS. G_{ant} and G_{FSS} are the gains of the transceiver and the FSS, respectively.

$$(S_{11}^{fab})^a = (S_{11}^{free})^b + (T_1 \Gamma_{FSS} T_2)^c \tag{6.2}$$

where a, b and c are unknowns. We believe that to correctly determine these constants, we need understand how the reflected fields from the FSS interact with the transceiver to give the total reflection coefficient.

Bibliography

[1] M. R. Andrews, P. P. Mitra, and R. deCarvalho. Tripling the capacity of wireless communications using electromagnetic polarization. *Nature*, 409:316–318, Jan. 2001.

[2] J. G. Proakis. *Digital Communications*. McGraw-Hill, international edition edition, 2001.

[3] G. J. Foschini and M. J. Gans. On Limits of Wireless Communications in a Fading Environment when Using Multiple Antennas. *Wireless Personal Communications*, 6(3):311–335, 1998.

[4] E. Telatar. Capacity of Multi-Antenna Gaussian Channels. *European Transactions on Telecommunications*, 10(6):585–595, Nov./Dec. 1999.

[5] B. A. Munk. *Frequency Selective Surfaces*. John Wiley and Sons, 2000.

[6] B. A. Munk. *Finite Antenna Arrays and FSS*. John Wiley and Sons, 2003.

[7] T. L. Marzetta. Fundamental Limitations on the Capacity of Wireless Links that Use Polarimetric Antenna Arrays. In *Proceedings of IEEE International Symposium on Information Theory*, page 51, Lausanne, Switzerland, Jun. 2002.

[8] A. S. Y. Poon, R. W. Brodersen, and D. N. C. Tse. Degrees of Freedom in Multiple-Antenna Channels: A Signal Space Approach. *IEEE Transactions on Information Theory*, 51(2):523–536, Feb. 2005.

[9] A. Nehorai and E. Paldi. Vector-Sensor Array Processing for Electromagnetic Source Localization. *IEEE Transactions on Signal Processing*, 42(2):376–398, Feb. 1994.

[10] D. D. Stancil, A. Berson, J. P. V. Hof, R. Negi, S. Sheth, and P. Patel. Doubling Wireless Channel Capacity Using Co-polarised, Co-located Electric and Magnetic Dipoles. *Electronic Letters*, 38(14):746–747, Jul. 2002.

[11] A. S. Konanur, K. Gosalia, S. H. Krishnamurthy, B. Hughes, and G. Lazzi. Increasing Wireless Channel Capacity Through MIMO Systems Employing Co-located Antennas. *IEEE Transactions on Microwave Theory and Techniques*, 53(6):1837–1844, Jun. 2005.

[12] A. Rajagopalan, G. Gupta, A. S. Konanur, B. Hughes, and G. Lazzi. Increasing Channel Capacity of an Ultrawideband MIMO System Using Vector Antennas. *IEEE Transactions on Antennas and Propagation*, 55(10):2880–2887, Oct. 2007.

[13] R. Heddergott and P. Truffer. Statistical Characteristics of Indoor Radio Propagation in NLOS Scenarios. Technical Report 259 TD(00), EURO-COST, Valencia, Spain, Jan. 2000.

[14] T. Zwick, C. Fischer, D. Didascalou, and W. Wiesbeck. A Stochastic Spatial Channel Model Based on Wave-Propagation Modeling. *IEEE Journal on Selected Areas in Communications*, 18(1):6–15, Jan. 2000.

[15] T. Zwick, C. Fischer, and W. Wiesbeck. A Stochastic Multipath Channel Model Including Path Directions for Indoor Environments. *IEEE Journal on Selected Areas in Communications*, 20(6):1178–1192, Aug. 2002.

[16] O. M. Bucci and G. Franceschetti. On the Degrees of Freedom of Scattered Fields. *IEEE Transactions on Antennas and Propagation*, 37(7):918–926, Jul. 1989.

[17] C. A. Balanis. *Antenna Theory: Design and Analysis.* New York: John Wiley and Sons, 2nd edition, 2002.

[18] W. L. Stutzman and G. A. Thiele. *Antenna Theory and Design.* John Wiley and Sons, 1981.

[19] C. H. Walter. *Traveling Wave Antennas.* Dover Publications Inc. New York, 1970.

[20] A. S. Konanur. *An Investigation on Vector Antennas.* PhD thesis, North Carolina State University, 2006.

[21] L. Zhu and K. Wu. Model-Based Characterization of CPS-Fed Printed Dipole for Innovative Design of Uniplanar Integrated Antenna. *IEEE Microwave and Guided Wave Letters*, 9(9):342–344, Sep. 1999.

[22] T. J. Warnagiris and T. J. Minardo. Performance of a Meandered Line as an Electrically Small Transmitting Antenna. *IEEE Transactions on Antennas and Propagation*, 46(12):1797–1801, Dec. 1998.

[23] Y. S. Seong, A. E. Waltho, L. Krishnamurthy, D. Souza, S. Gupta, H. K. Pan, and V. K. Nair. A Miniaturized Dual-band Dipole Antenna With a Modified Meander Line for Laptop Computer Application in the 2.5 and 5.25 GHz WLAN band. In *Proceedings of IEEE Antennas and Propagation Society International Symposium*, pages 2617–2620, Jul. 2006.

[24] S. Krishnamurthy, A. Konanur, K. Gosalia, G. Lazzi, and B. L. Hughes. On the Impact of Polarimetric Vector Antennas in Wireless Communications. In *2003 Conference on Information Sciences and Systems*. The Johns Hopkins University, Mar. 12-14 2003.

[25] S. H. Krishnamurthy, A. S. Konanur, G. Lazzi, and B. L. Hughes. On the Capacity of Vector Antenna MIMO Systems. In *Internation Symposium on Information Theory*, page 243, 2004.

[26] H. Hashemi. The Indoor Radio Propagation Channel. *Proceedings of the IEEE*, 81(7):943–968, Jul. 1993.

[27] R. B. Ertel, P. Cardieri, K. W. Sowerby, T. S. Rappaport, and J. H. Reed. Overview of Spatial Channel Models for Antenna Array Communication Systems. *IEEE Personal Communications*, 5(1):10–22, Feb. 1998.

[28] M. C. Mtumbuka and D. J. Edwards. Investigation of Tri-polarised MIMO Technique. *Electronics Letters*, 41(3):137138, Feb. 2005.

[29] M. C. Mtumbuka, W. Q. Malik, C. J. Stevens, and D. J. Edwards. A Tri-polarized Ultra-wideband MIMO System. In *IEEE/Sarnoff Symposium on Advances in Wired and Wireless Communications*, pages 98–101, Apr. 2005.

[30] L. C. Godara. Application of Antenna Arrays to Mobile Communications, Part II: Beam-forming and Direction of Arrival Considerations. *Proceedings of the IEEE*, 85(8):1195–1245, Aug. 1997.